11-13-2003

Parametric modeling of tooling: Workpiece interaction with engineered abrasives

Hitesh Kataria

Parametric Modeling of Tooling –Workpiece Interaction with Engineered Abrasives

Date: 13th November 2003

Graduate Student

Hitesh Kataria

Industrial and Systems Engineering Department
Rochester Institute of Technology

Committee Members

Dr. Andres Carrano

Chair Assistant Professor

Industrial and Systems Engineering.
Kate Gleason College of Engineering.

Dr. Brian Thorn

Associate Professor

Industrial and Systems Engineering.
Kate Gleason College of Engineering.

REPRODUCTION PERMISSION STATEMENT

PERMISSION DENIED

Parametric Modeling of Tooling –Workpiece Interaction with Engineered Abrasives

I, Hitesh Kataria, hereby deny permission **to any individual or organization to reproduce this thesis in whole or in part.**

Hitesh Kataria

3rd February 2004

Date

KATE GLEASON COLLEGE OF ENGINERRING

ROCHESTER INSTITUTE OF TECHNOLOGY

ROCHESTER, NEW YORK.

CERTIFICATE OF APPROVAL

MASTER OF SCIENCE DEGREE THESIS

The M. S. Degree Thesis of Hitesh C. Kataria
has been examined and approved by the thesis committee
as satisfactory for the thesis requirement for the
Master of Science degree.

Dr. Andres Carrano, Ph.D. Advisor

Dr. Brian Thorn, Ph.D.

Acknowledgements

I would like to express sincere thanks and gratitude to my graduate advisor, Dr. Andres Carrano for his relentless help, support, and motivation. I would also like to thank him for giving me an opportunity to work as a research assistant during my course of study and for providing me with financial support throughout my course at RIT. I am truly grateful to him for his understanding and encouragement and patience with my shortcomings. I am sure that he would truly remain an inspiration for the future generations.

My deepest thanks to the Industrial and Systems Engineering Department for having me as a part of the RIT culture and for providing an excellent platform to launch my career in the field of Industrial Engineering.

My heart-felt gratitude also goes out to all the professors and the staff in the Industrial and Systems Engineering department. A special thanks to Dr. Brian Thorn for being a part of my thesis committee and for guiding me to complete my thesis work.

My sincere love and thanks to my family for their motivation and support that allowed me to travel half way across the world to RIT for my Masters. A special thanks to my sister Sonali without whom this venture would not have been possible.

ABSTRACT

Abrasive processes are some of the most important operations employed in manufacturing to remove unwanted material and introduce desired geometry and surface finish. However, some of the difficulties encountered when trying to model abrasive process are related to a multi-point of contact tooling composed of extremely hard and brittle particles which geometry, shape and distribution are unknown. With the introduction of engineered abrasives to the market over the past few years, the opportunity to drastically improve the quality and consistency of abrasive machining now exists. One of the main benefits of engineered abrasives is the ability to control the abrasive grit properties i.e. size, shape, distribution and composition. The objective of this study was to develop a parametric model of the engineered abrasives that allows for studying the interaction of this particular tooling with various surfaces. This would also allow for prediction of surface roughness from a given tool-workpiece pair. The development of this model, the analysis of the tool-workpiece interaction, and the algorithms for surface generation are carried out using a computer model developed for each specific purpose. Additionally, experimental validation of this model is presented. It was found that the machined surface improves as the depth of indentation increases, but beyond a certain level the surface roughness obtained becomes asymptotic. It is observed that machining at 30° attack angle results in the smoothest surface and that increasing the number of abrasive grits beyond a certain number does not yield better surface. Contributions of this project include suggestions for new tooling geometry for abrasive manufacturing and optimization of machining parameters for efficient operations along with a simulation tool for a better understanding of the abrasive machining process.

TABLE OF CONTENTS

LIST OF TABLES

Page

LIST OF FIGURES

Page

1.INTRODUCTION

Metal or wood parts rarely obtain their final finish through manufacturing process such as casting, forging and machining. Secondary processes such as grinding and polishing are normally used to give the object their final smooth form. These processes are commonly known as abrasive machining processes.

Abrasives are used with hard materials, such as metals and ceramics that are too hard or too tough to be machined by single point tool. Another important application of abrasive process is when a good surface finish or highly polished surface is required. Metal and ceramic grinding and wood sanding are some of the biggest application for abrasives. Some abrasives occur in nature (flint, garnet, etc), and some are man-made (aluminum oxide, silicon carbide, zirconia, etc). Until now, most coated abrasive tools have consisted of single or multiple layers of oriented grits of approximately the same size that are attached to a substrate. The size of the particles used on coated abrasives is established by passing the crushed grits through screens of standard mesh [58] while some of the finest grit sizes are segregated by sedimentation or air floatation. The application of the abrasive grits to the belt backings are either achieved through gravity or electrode-induced polarization. This traditional manufacturing practice, however, yields an abrasive belt that presents variations in grit size, grit distribution, and grit orientation.

The machining process is generally not as understood as it appears. One of the common issues that arise in abrasive machining of wood is the inconsistency of the surface roughness under identical machining parameters. In abrasive machining processes, not all points are in contact with the workpiece at any given time and the dynamics of the processes and the structure of the abrasives normally cause these active points to fracture.

This ongoing fracture mechanism generates new, perhaps unpredictable, geometries in active particles or lowers their profile sufficiently so other neighboring particles become active. Additional difficulties encountered are the multi-point of contact tool composed of small, extremely hard, and brittle refractory particles whose geometry, shape, and distribution are unknown. Because of all these mechanisms, the geometry of cutting grits changes from particle to particle, making it impossible to know, for instance, the rake or attack angle for any given grit and cut. All these phenomena make it even more difficult to model this abrasive machining process.

Abrasive-based machining processes have been some of the most difficult and challenging to model and characterize. Earlier efforts have included models assuming single point cutting tools with known geometry, as well as statistical input-output characterization via experimental design. But none of these models have tried to incorporate the abrasive machining processes as a multilayer or continuous process nor do they model this as a closed form. The single grit tooling assumption simplifies the model but is not realistic. It has been difficult to understand from this model the effects of multiple passes and the effects of multiple grits on workpiece surface.

Recent advances in manufacturing processes have allowed replacement of the random arrangement of minerals on conventional belts by a technology called *microreplication.* 3M defines microreplication as, the science of creating small, precisely shaped, three-dimensional structures and reproducing them on a variety of surfaces. The belt's surface, considered in this case, consists of precisely shaped pyramidal structures containing micron-graded minerals that are uniformly applied to a backing material. This development has been around for several years but it was not until recently that

commercial fabrication of belts became feasible. The new class of abrasive tools is called *engineered or structured abrasives.* They consist of abrasive belts that are more deterministic: the shape, size, distribution and orientation are known and controlled. This provides a very even distribution of mineral and yields a more consistent rate of cut and surface finish. The motivation for making such abrasives lies in the idea that, by removing variation in the grit geometry, it is possible to remove variation in the finish quality.

A 3D model that can simulate the geometric features of the engineered abrasives can help in better visualization and understanding of these abrasives. A model that possesses the ability to manipulate the geometric parameters of these abrasives can help determine the optimized geometry for a particular surface roughness. Such a model is presently not available for analysis. The development of computer models that can simulate and replicate the engineered abrasives is believed to support future advance such as custom-patterned abrasives, etc.

1.1 STATEMENT OF RESEARCH

The motivation behind developing an abrasive tool model is to provide a better insight of the impact of the individual geometric features of abrasives on surface roughness. By doing this, new geometries that would perform better can be proposed. The hypothesis is that, by varying each parameter involved in the abrasive machining processes and studying their effect on the machined surface it is possible to predict the resultant surface as well as to optimize the process and tool parameters. Furthermore, developing a

parametric tool coupled with a workpiece surface model will help researchers characterize and understand the abrasive machining process.

The proposed study has been subdivided into four main areas:

- **Parametric modeling of abrasive tooling:**

  The objective of this part is to develop a geometric tool that would allow defining and manipulating the different shape parameters and properties of the engineered abrasives while generating various tooling configurations. The developed model would help in visualizing abrasives in 2D and 3D and lead to a better understanding of the impact of their geometry during machining in this section. The parameters of interest are the size, shape and distribution of the abrasive grits as well as their relative orientation with respect to the feed direction. Since it was the first commercially available configuration, this study focuses exclusively on pyramid-shaped grits with rectangular base.

- **Generation of workpiece surface:**

  The objective of this section is to develop a model capable of representing many different surface roughnesses prior to machining. The parameters of the discrete data composing the roughness distributions are obtained via reverse metrology from specimens machined in controlled experiments. Consequently, these computer-generated surfaces are developed to resemble the actual ones.

- **Modeling of tooling-workpiece interaction:**

  This section combines the earlier two outputs to develop the interaction between the tool and the generated surfaces. This interaction is graphically generated on the

computer and the resultant profile after machining is then assessed. Calculations of the corresponding surface descriptors are obtained and compared against available experimental values.

- **Experimental validation and contribution:**

  Experimental validation of the created program is carried out in this section. A set of previous experiments that were created using known geometric parameters of the abrasives (such as their width and height, the attack angle, etc) is used. The relevant surface from the experiments is assessed and documented. These results are then validated against the output from the computer model under identical conditions for verification purposes.

2.BACKGROUND

2.1 Fundamentals of coated abrasives

Coated abrasive products have been used for a long time as a highly efficient method of metal removal and finishing. The construction of these coated abrasives has been relatively standard: a flexible or semi rigid backing to which a single or multiple layer of abrasive grain is randomly arranged and bonded by an adhesive. They are constructed by combining minerals, backings and bonds to form the products.

Abrasive minerals perform the basic operation of grinding, cutting, etc. Some of these abrasives occur in nature (emery, garnet) whereas some are synthetically manufactured (aluminum oxide, silicon carbide). Backings are the substrate, which carry and support the mineral grains. Some of the backings used include paper, cloth, and fiber, among others. These abrasive grits are bonded by glue, resin over glue, or resin over resin. The abrasives are then applied to the backing by gravity coating process in which the abrasives are dropped from an overhead hopper onto the backing. Another method is electrostatic coating process in which, the backing is coated with an adhesive bond and the abrasive grains pass through an electrically charged field. As the abrasive grains and the coated backing pass simultaneously through the electrostatic field, the abrasive grains are propelled upward and embedded in the adhesive on the backing. The size of the particles used on coated abrasives is established by sifting the crushed grits through screens of standard mesh [58]. Some of these grits are segregated by sedimentation or air floatation. This traditional manufacturing process, however, results in an abrasive belt having inconsistent grit size, grit distribution, and grit orientation. The nature of this

process does not allow for accurate control of the contact area between abrasive grain and the workpiece for a given pressure, and may result in an unexpected finish.

Recent advances have been made in the manufacturing processes of abrasives and a new technology called '*microreplication*' has been developed. 3M Corporation defines microreplication as, the science of creating small, precisely shaped, three-dimensional structures (e.g. pyramids, cones etc) and reproducing them on a variety of surfaces. Multiple patterns of these structures provide more options for achieving the best grinding results. This new class of abrasives is known as '*engineered or structured abrasives*'. (Fig. 2-1)

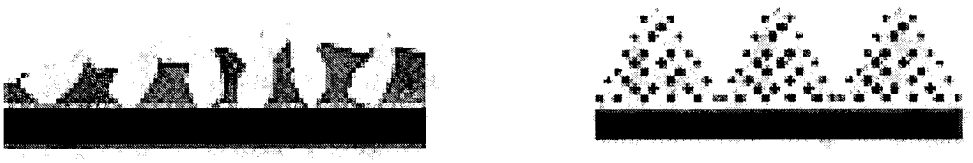

Conventional Abrasive **Engineered Abrasive**

Fig. 2-1: Conventional and engineered abrasives.

These abrasive belts are more deterministic: the shape, size, distribution and orientation are known and controlled. It is claimed that they offer performance gains such as higher stock removal rate, improved surface finish, and increased belt or disk life by 3-10 times. As the 3D structures are worn in the grinding process, successive layers of fresh cutting points are exposed. Additionally these new abrasives are reported to provide cooler cutting, resulting in less metallurgical damage to the part. Engineered abrasives are narrow belts available with aluminum oxide and silicon carbide abrasives in grit sizes comparable to conventional abrasives ranging from P150 to P2500. Backings are either

flexible cotton or semi-rigid polyester. Currently there are three abrasive patterns available: Pyramid, Quad and Tri-helical, as shown in figure 2-2.

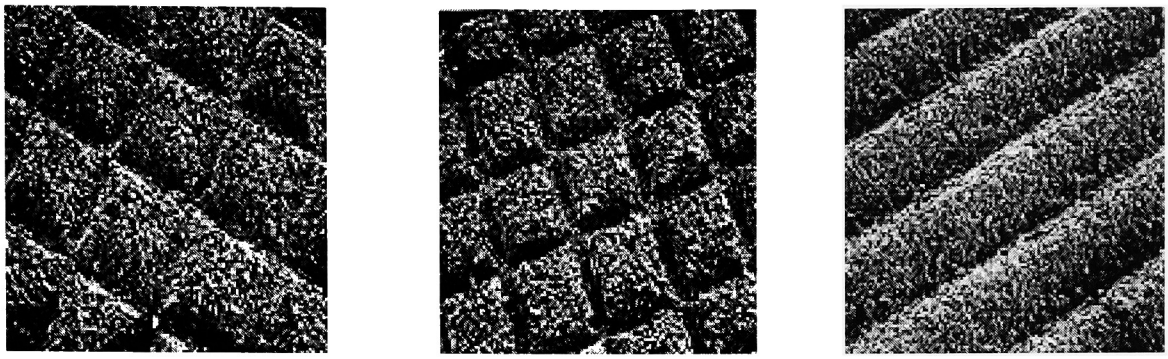

Pyramid **Quad** **Tri-Helical**

Fig 2-2: Engineered abrasive Patterns (Source: www.nortonabrasives.com)

This study focused on the pyramid shaped engineered abrasives.

2.2 Fundamentals of abrasive machining process.

In general, an abrasive machining process is not 100 percent efficient. This is due to the fact that the volume of workpiece swept by the tool is not completely removed. The process is extremely complex, because of the irregular shape of abrasive particles. Only a portion of such particles actually cuts into the metal. The shape of the abrasive particles, that cut the metal, determine the profile of the machined surface. The rest of the particles either scratch the surface or pass over it without making contact with the workpiece. The rake angle and the geometry of the abrasive particles are some of the parameters, which determine the final machined surface roughness. The rake angle (the angle between the advancing face of the pyramid and a vertical line perpendicular to workpiece surface) is one of the most significant parameters in abrasive machining. (Fig. 2-3)

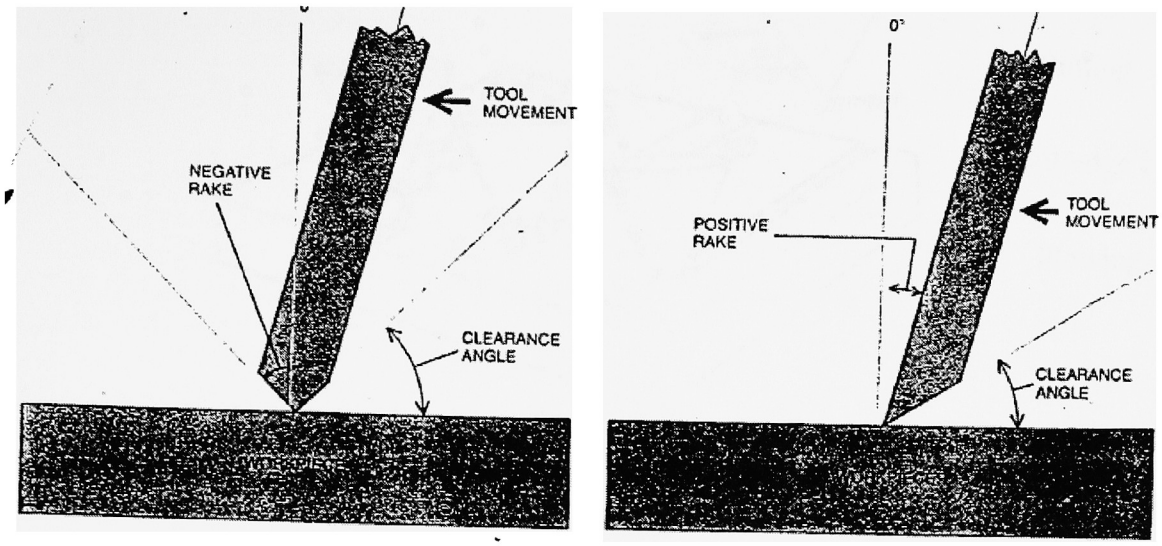

Fig 2-3: Negative and positive rake angle. (Source [46])

Grooves produced by pyramids that have negative rake angles usually terminate with a long, ribbon like chip. It can be assumed that all the volume of workpiece material swept by the point is now in this chip and that all the material would be removed from the work piece if the chip broke off. The chip will eventually break off, when the tool reaches the edge of the workpiece. The point can be assumed to be operating in cutting mode.

Grooves that have been produced by pyramidal points with positive rake angles usually terminate in a prow. Ridges form at each side of the groove, so that the size of the prow is constant no mater how far the point has moved. The volume of material swept out in the workpiece by the point is now in the prow and the ridges. The point is operating in a plowing mode, and the efficiency of removal of material is zero unless the prow or the ridges break off.

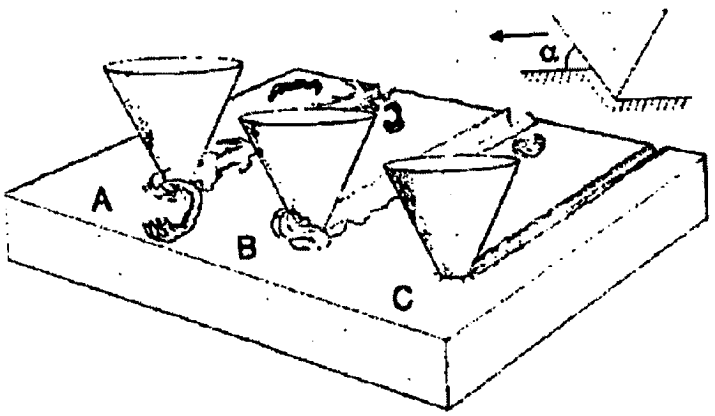

A - Cutting

B – Wedge Forming

C - Plowing

Fig 2-4: Wear modes in single tip grooving. (Source [21])

In cutting mode the material moves continuously upward past the rake face of the tool, separating a ribbon of material from the surface. (Fig.2-4). In wedge forming, the abraded material is pushed in front of the tip, producing a wedge-like wear particle which continuously grows and eventually falls off, the wedge works as a built-up edge. In plowing mode, material first moves in advance of the rake face and then moves around the face into the side ridges, resembling the bow wave formed in front of a ship. The important point is that material is merely moved on the surface but is not detached. It can be moved through some secondary process. The implication is that the efficiency of removal of material in an abrasive machining process will be determined by the proportion of abrasive points in contact with the workpiece that have a rake angle suitable for cutting a chip.

Another important factor in the efficiency of abrasion is the value of the critical rake angle. Critical rake angle is the angle that is the dividing line between efficient and inefficient removal of material. The more negative the angle, the larger the proportion of the points in an abrasive paper that will cut a chip. The value of the critical angle is also

dependent on the workpiece material but at present it is not possible to say categorically which basic properties of the material determine the value of the critical angle [46].

2.3 Fundamentals of numerical methods and statistics

2.3.1 Newton Raphson method

Whenever the roots of a non-linear equation f (X) = 0 cannot be found in a closed form, it is necessary to resort to approximation methods. Such methods are iterative, i.e. start from X_0, X_1, X_2 .. and converge to a desired root.

The roots of an equation are those values of some parameters for which the equation is satisfied. Numerical methods are used to approximate these roots. In the present case, the non-linear expression is a polynomial equation of high order. Approximation methods are used in this work to approximate the roots that satisfy the intersection between a line and polynomial equation. These roots represent the points of intersections between the two equations (shown later) and are used to determine the profile of the machined surface.

Numerical methods are iterative algorithms for finding a numerical quantity to a prescribed accuracy. It is a mathematical procedure, which reaches its solution in a step-by-step fashion. These methods give solutions through successive and iterative calculations. Newton Raphson method is the numerical method used to approximate the roots in this case.

The Newton Raphson Method is defined by:

$$X_{n+1} = X_n - \frac{f(x)}{f'(x)}$$

Where f' (x) is the first derivative of the function f(x).

Starting with a given initial approximation X_0, a sequence X_1, X_2, X_3... is computed, where X_{n+1} is determined by the aforementioned formula. The function f(x) is approximated by its tangent at the point $(X_n, f(X_n))$, and X_{n+1} is taken as the abscissa of the point of intersection of the tangent with the x-axis.

If $f'(x) = 0$, or even if $f'(x) = 0$ for x near $\bar{x}$ (where $\bar{x}$ is the root), then there may be some trouble locating $\bar{x}$. Some of the possible difficulties are illustrated in Figure 2-5.

The problem in Figure 2-5, (a) – (c) arises because the graph of f has a running point (local max or local min) near the x –axis. When this occurs, it, may not be clear from a rough sketch whether the x – axis is touched at a single tangency point x (a), at two close interval x1 and x2 (b), or not at all (c). In case (d) there is a root, but it is hard to say exactly where.

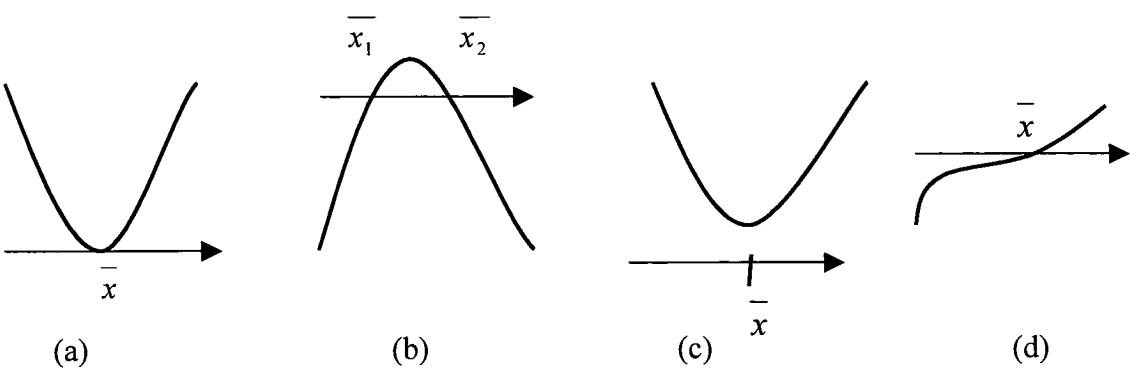

Fig 2-5: Situations that present numerical difficulties to finding roots. (Source [37])

For all cases a through d, the following applies:

Both $f(x) = 0$ and $f'(x) = 0$ for $x \approx \bar{x}$

For such x, round off error (due to loss of significance) in calculating $f(x)$ can be greater than $|f(x)|$ itself, making $f(x)$ hard to evaluate accurately. As a result, all root-finding methods will have difficulty finding $\bar{x}$ accurately.

2.3.2 Monte Carlo simulation

The Monte Carlo simulation method consists of a simple structure of computational algorithm. This algorithm consists, in general, of a process for producing random events. The process is repeated N times, each trial being independent of the rest and with the results of all trials averaged together. Because of its similarity to the process of performing a scientific experiment, the Monte Carlo method is sometimes called the *method of statistical trials*. In a more strict sense of the term, the Monte Carlo method is defined as the construction of an artificial random process possessing all the necessary properties, but which is in principle realizable by means of ordinary computational apparatus: pencil, paper, tables, computers and sometimes simple apparatus for generating random numbers. (Such as a table of random numbers).

Problems handled by Monte Carlo methods are either called probabilistic or deterministic according to whether or not they are directly concerned with the behavior and outcome of the random processes.

In the case of probabilistic problem the simplest Monte Carlo approach is to observe random numbers, chosen in such a way that they directly simulate the physical random processes of the original problem, and to infer the desired solution from the behavior of these random numbers.

In the parametric model developed here, the probabilistic approach of Monte Carlo simulation is used during the workpiece surface generation. N random numbers are generated using gamma distributions, which were assumed to be representative of the properties and roughness parameters of the original surface. These numbers are then fitted with a polynomial curve and the random numbers now represent a workpiece

surface that can be machined by the tool. This process is carried out N number of times (10,000 in the case of this work) to incorporate the inherent randomness of surface roughness. Each time the surface is machined, the roughness parameters of the machined surface are calculated. An average of these parameters is taken to calculate the final result. This methods usually allows for confidence intervals to be calculated for the data generated.

2.3.3 Random number generation

Random numbers are needed in a wide range of areas, such as Monte Carlo methods, but they are also of great importance in computational statistics, in the implementation of probabilistic algorithms, and in related problems of scientific computing. In addition, random numbers are applied in areas of direct practical interest such as VLSI testing, cryptography, and computer games. Given a distribution function F on $\Re$ random number generators introduce a sequence of real numbers that simulates a sequence of independent and identically distributed random variables with a distribution function F.

Early in the history of the Monte Carlo method, it became clear that in the case of sequences generated by computers "truly random" numbers are fictitious from a practical point of view. Hence pseudorandom numbers (abbreviated PRN) can be generated by the computer using deterministic algorithms with relatively few input parameters. The standard algorithms for generating sequences of PRN are based on recursive procedures and yield sequences that are ultimately periodic.

Furthermore there are two types of pseudorandom numbers, *uniform pseudorandom numbers* and *non-uniform pseudorandom numbers*. The task in uniform PRN - generation

is to generate a sequence of real numbers that simulates a sequence of independent uniformly distributed random variables in [0,1]. Non-uniform PRN's are obtained by transforming uniform PRN's to a given distribution. Many methods have been developed for transforming uniform PRN into non-uniform PRN; some of them are as follows:

(i) Inversion method: Where the uniform PRN function F has an inverse function F^{-1} defined as the non-uniform PRN.

(ii) Rejection method: Where the random number generated are accepted or rejected based on the comparison of certain condition.

(iii) Composition method.

(iv) Ratio-of-uniforms method.

There are quite a few other general techniques for transforming uniform PRN into non uniform PRN, and there is a great abundance of methods tailored to special distributions, such as normal distributions, beta distributions, gamma distributions, and so on.

For the parametric model a gamma distribution is used to generate pseudo random numbers. The scale and shape parameter of the gamma distribution are used to generate PRN. The gamma distribution was used in this case because it relies on two parameters sample (skewness & std. deviation) to calculate its shape and scale parameter, which in turn are used to generate PRN.

The formula for PRN using gamma distribution is:

$$\Gamma{:}b,c \sim -b\log(\Pi R_i) = \sum -b\log R_i$$

Where R_i – independent unit rectangular variates.

b - scale parameter

c - shape parameter

2.3.4 Gamma distribution

The gamma distribution produces the chi-squared, Erlang, and exponential distributions as special cases, but the shape parameter of the gamma is not confined to integer values. The gamma distribution starts at the origin and has a flexible shape. The parameters are easy to estimate by matching moments.

Variate γ:

Parameter: b (scale), and c (shape).

Range $0 \leq x < \infty$.

Scale parameter $b > 0$.

Shape parameter $c > 0$.

Probability density function: $\left(\frac{x}{b}\right)^{c-1} \frac{\left[\exp\frac{-x}{b}\right]}{b\Gamma(c)}$

Where $\Gamma(c)$ is the gamma function with argument c.

Mean: bc

Variance: b^2c

Coefficient of skewness: $2c^{-1/2}$

Coefficient of kurtosis: $3+\frac{6}{c}$

Special cases of the gamma variates exists:

These variates,

1. **Exponential variates E:**

Variate **E**: b

Scale parameter $b > 0$, the mean

2. Weibull variates W:

Variates **W**: b, c

Scale parameter b > 0,

Shape parameter c > 0

3. Erlang Distribution:

Variates γ: b, c

Scale parameter b > 0,

Shape parameter c > 0

4. Chi-squared variates X^2:

Variates X^2: v

$b = 2$

$c = v/2$

Shape parameter v, degrees of freedom.

2.4 Literature review

Some of the literature review in the areas of abrasive machining, and surface roughness is presented in this section. A classical paper titled "Machining Wood with Coated Abrasives" [17] presented the effects of standard parameters such as pressure, belt speed, contact area, moisture content and dressing with respect to material removal rate, power consumption and belt life. This research is still one of the most exhaustive efforts completed in this area, though it is more than four decades since it was published. Some limitations in this study were: input-output relationships were analyzed in a one-at-a-time fashion (no interactions considered); no surface pattern or quality was observed as an output and abrasive minerals as well as grit size range were limited to those used at that time. Additional work in this area of process parameters was done by Stewart [53], in which all-possible combinations of three parameters (grit size, mineral type, and platen pressure) at three levels were considered. In this case, the experiment was performed on a stroke sander under dynamic conditions. The material removal rate was the only response observed. Terry and Brown [56] investigated the parameters for characterizing topographies and a method of selecting these parameters. Conventional and scale-sensitive fractal parameters were tested for cross-correlation, ability to differentiate process variables and ability to relate grinding wheel topography with ground surface topography. It was found that no parameter could differentiate the process variables or could relate wheel and workpiece topographies in all situations. The waviness height (Wt) was the best for differentiating process variables, and a scale-sensitive fractal-based parameter, the smooth-rough crossover (SRC), was best at relating workpiece and wheel topographies. The work by Carrano [8] and by Taylor, Carrano, Lemaster [55] represents

two of the very few attempts to characterize multiple parameters. In these studies, the main effects, interactions, and response surfaces of grit size, interface pressure, abrasive mineral, and grain orientation are presented with respect to material removal rate and surface roughness. Some of the results indicate that silicon carbide produce a better surface than aluminum oxide, this being more pronounced when using coarse grit sizes. Additionally, two and three factor interactions were negligible for all grit sizes studied. Some studies on abrasive metal machining have provided insights into the process. The work by Mulhearn and Samuels [38], and Samuels [45] addressed several aspects of the abrasion of metals in metallographic polishing process. Initially, a distribution curve for rake/attack angles for a two-dimensional case was developed. It was found that there is a well-defined attack angle above which the point cuts a chip, but below this threshold, it merely ploughs a groove. For steel, this critical angle was determined to be 90° and that only about 20 percent of the contacting points in a 220-grade silicon carbide paper would cut a chip. Additionally, scanning electron microscopy revealed that the development of flats at the contact tips by means of attrition wear was negligible. However it was also found that the fracture mechanisms were of much greater significance. Such fractures characteristically followed a plane perpendicular to the rake surface of the abrasive particle (plane of principal stress) if there are no pre-existing cracks on the abrasive surface. This indicates that contacting points, which initially were shaped so that they rubbed a groove, will continue to do so after the point has fractured. However, contacting points that initially ploughed are likely to remain ploughing points if the attack angle was less than 90°, but are likely to become rubbing points if the attack angle was greater than 90°. Finally, this work also examined how the number of contacting particles increases

with the use of the paper. Buttery and Hamed [6] developed a geometric representation of cutting by single grit based on the scratch pattern. This was derived for a Vickers pyramid indenter with the known geometry and was verified experimentally on carbon steel with a surface grinder.

Gahlin and Jacobson [21] worked on the influence of tip angle, tip blunting and tip packing density on the wear rate. Wear tests were performed in a pin-on-abrasive disk configuration with tin as abraded material. It was found that the angle dependence of the abrasion rate is approximately linear and independent of the packing density of the tips. Blunt tips, however, gave lower rates and also lower sensitivity to variation in the tip angle than sharp tips. Further, the sensitivity of the tip angles fell with increased packing density of the tips. Gahlin and Jacobson [22] researched the particle size effect in abrasion by controlled abrasive surfaces. In this work, abrasive surfaces were created by using a micro-mechanical etching technique, which allows for manufacturing different packing densities and tip radius. It was found that blunt particles exhibit a size effect while sharp particles do not. In those situations where wear debris accumulated on the abrasive surface, clogging also resulted in a particle size effect. Other small differences (such as pyramid angle) showed a strong impact on the wear rate. The work by Komanduri and Shaw [30] attempt to explain the differences in performance among commercial abrasives used in grinding by means of topography observations in a scanning electron microscope. Here, some relationships between surface morphology and structural defects with respect to grinding performance were developed. Komanduri [29] discussed how the rake angles and the widths of cut are the parameters determining the transition between cutting a chip and ploughing a groove. In this work, the importance of

frictional conditions at the rake angle face on the previously mentioned transition is also discussed. Some work in modeling this process [42] has also been developed based on slipline field theory. Gahlin and Jacobson [18] studied the effects of high biaxial compressive stresses on the abrasion of diamond coatings by diamond particles. It was seen that the highly stressed coatings obtained a smoother worn surface and a significantly lower wear rate as compared to the stress-free coatings. It was found that biaxial stresses increased the inherently high wear resistance of diamond coatings. Gahlin and Jacobson [19] developed an etching procedure to produce silicon abrasive surfaces in a controlled and reproducible way. The process developed was successful in manufacturing well-defined abrasive surfaces in silicon showing nearly constant tip shape and size over large areas. Gahlin and Jacobson [20] developed two new techniques for wear evaluation on a micro-scale: local wear volume determination and wear distribution mapping. These techniques were based on studies of the same surface area before and after wear. Ulf [57] showed the applicability of light as a means of controlling the surface roughness in a grinding process. The specular reflected light increases as the surface is smoothened.

Clearly, the introduction of engineered abrasives as a new tooling presents a unique opportunity for both modeling and validating the abrasive process. To date most studies have addressed single grit models. A gap in current research exists related to the multiple pass effects and effects of the individual tooling geometry upon final machined surface. To develop better and more efficient engineered abrasives, an understanding of the way in which the tooling affects the final roughness of the machined workpiece is required. The objective of this study is to address this gap.

3. METHODOLOGY

3.1 Parametric modeling of abrasive tooling

The first commercially available engineered abrasives presented pyramid-shaped grits with rectangular base. These pyramidal structures can be characterized with two base widths and a height. The proposed tooling model is generated by varying the geometric parameters such as the base widths, and the pattern of these pyramidal shaped abrasive grits. The model is generated with information from a micrograph of an actual abrasive sheet. As seen in Figure 3-1, base widths of the pyramid shaped tool are mapped into a computer representation shown on the right. These dimensions of the geometric parameters are measured from the micrograph using Sigma Scan Pro® software and used as input to develop the tooling model.

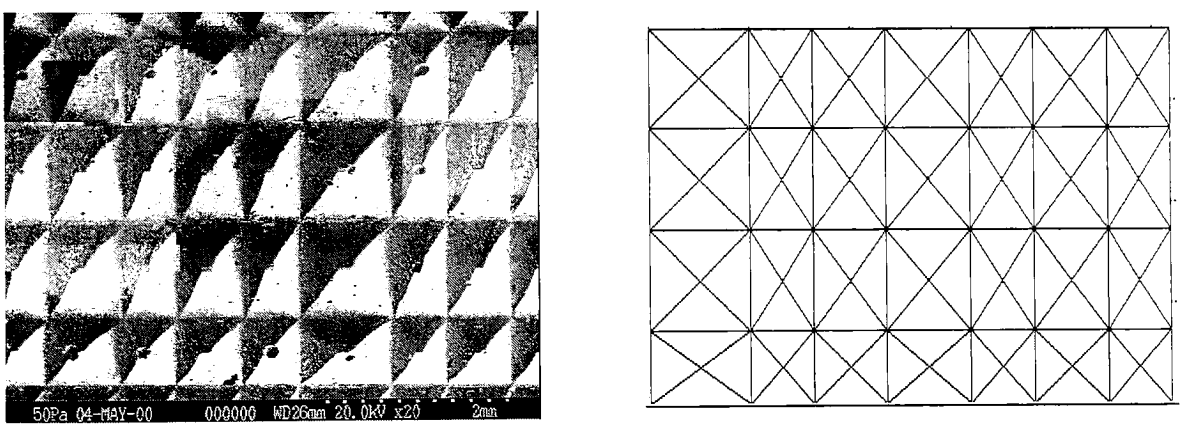

Fig 3-1: Micrograph of pyramidal grits and tool model representation.

Due to the nature of the manufacturing process that produces these abrasives, a patch defining the basic tooling matrix is then developed. This patch is replicated throughout the entire belt surface. It consists of a 7 x 4 pyramid grits matrix as shown in Figure 3-1. For convenience the rectangular base widths of each of the 28 pyramid grit vary along the X-axis and Y-axis of a standard cartesian 3 dimensional axis configuration. The Z-axis

represents the height of the grits (not shown). Two *Vectors of change* are then defined from the micrograph measurements. A vector of change is a ratio used to manipulate the X and Y dimensions of each grit with respect to a base grit (of ideal dimensions 1 by 1 units). It consists of two vectors A (7 X 1) and (4 X 1) as follows: (1, 0.63, 0.72, 0.83, 0.74, 0.63, 1) for X-axis and (1,0.72, 0.72, 0.72) for Y-axis. This vector was developed from measurements taken from the micrograph. The path size can be assumed either as standard, thus replicating the micrograph or scaled for e.g. 0.5 times the original patch size. (This would reduce the base widths in both the X-axis and Y-axis by half). This ratio can be changed as desired. The patch can then be replicated (N) number of times in rows, (number of patch rows X 4 rows in a patch) and (M) number of times in columns, (number of patch columns X 7 columns in a patch) thus resulting in multiple grit tooling environment simulation. The scale is selected such that the dimensions of the pyramidal grits in the model are equal to the dimensions of the grits in the micrograph. It gives an opportunity to simulate a condition where the base widths are increased or decreased as desired at the same time keeping the aspect ratio of the base widths constant. To incorporate feed direction, the tooling model can be rotated at a specified angle (attack angles, the angle at which the tool machines the surface) about Z-axis (Fig.3-2) Homogeneous transformation are used to rotate the coordinates of the pyramid grits to the specified angle about Z. The homogeneous transformation used is presented below (α indicates attack angle).

$$T(\alpha) = \begin{bmatrix} \cos\alpha & -\sin\alpha & 0 & 0 \\ \sin\alpha & \cos\alpha & 0 & 0 \\ 0 & 0 & 1 & 0 \\ 0 & 0 & 0 & 1 \end{bmatrix}$$

To provide perspective view of the pyramid grits, the abrasive tooling is represented in 3D (Fig.3-2). To visualize the machining process in 2D, the tooling model is projected on the XY (top view) plane and XZ (side view) plane. Figure 3-2 shows a 3D view of a particular tool configuration. It shows a patch size of 1 x 1, which includes 7 grits/row and 4 rows at 35° attack angle. The XY projection gives a better understanding of the base widths and the patch size while the projection in XZ provided the cumulative profile of the tooling as it approaches the surface and represents the multiple pass effect that effectively occurs during machining. This projection (XZ) is used to develop the algorithm for the tooling-workpiece interaction.

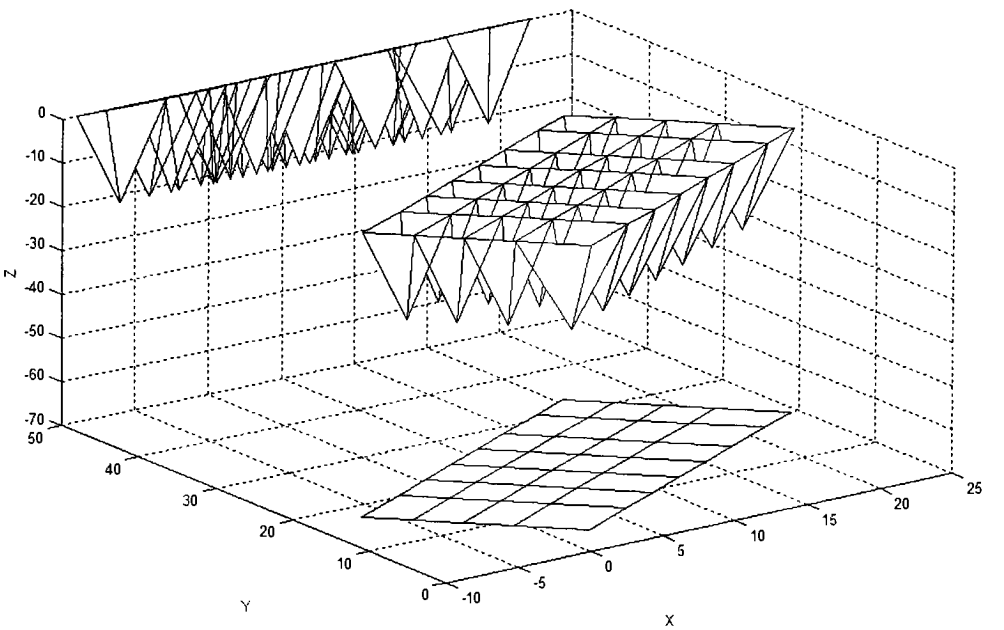

Fig 3-2: 3D image of tooling model with projections in XY and XZ plane.

Figure 3-3 shows a 2D view of the tool projection in XZ plane. The projection in this example is of a tool at 35° attack angle and patch size of 2 x 1.

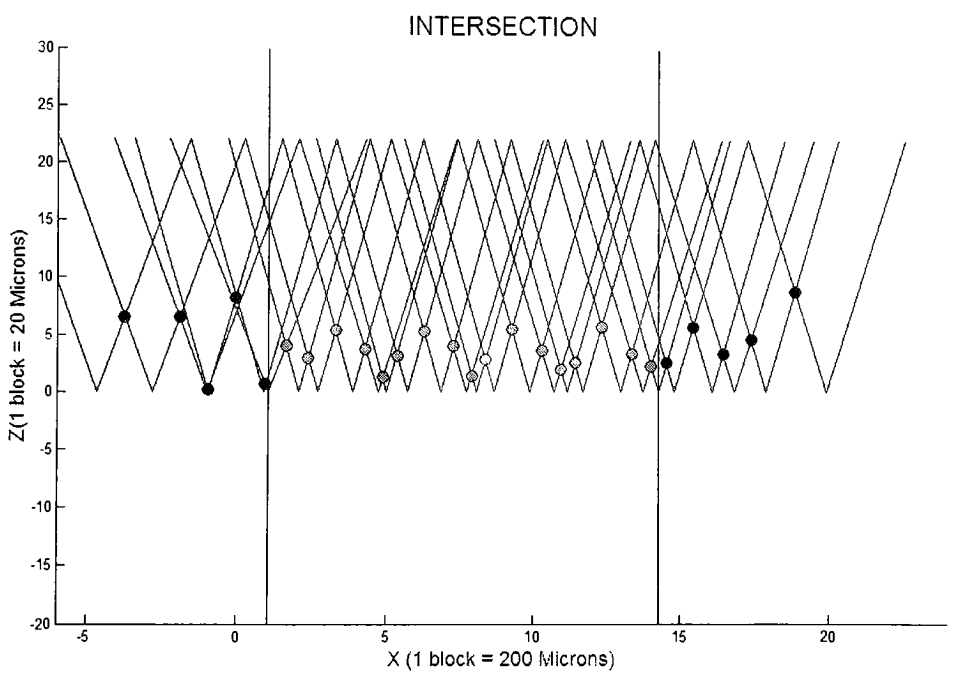

Fig 3-3: 2D projection of the pyramid grits in the XZ plane.

Certain assumptions had to be established when developing this model. These are:

- All rows must have same number of abrasive grits.
- The volume removed is the volume swept by the portion of pyramids that is underneath the work surface. (100 % efficiency [45] [46]).
- The feed direction is always parallel to the Y-axis.
- Rotation must be limited between 0° and 45°. Beyond 45°, other vertices will give the projection of grits without producing different projections.
- The geometry of the grits must be kept without change, i.e. there is no crushing, fracturing, cracking, or wear of any kind of the grits.

An important circumstance that has to be considered to keep the model realistic: the entire projection length is never swept by all rows of grits. Consequently, it is not possible to use the total projection length as the evaluation length for descriptor calculation.

It was necessary to develop an algorithm that would calculate the section of the projected length that was swept by all rows (so called evaluation length) to be used for further calculations (Fig 3-4). This algorithm would calculate the leftmost vertex (or closest to the Y-axis) from the first grit on the last row (this is grit (M, 1)) and the rightmost vertex (or farthest from Y-axis) from the last grit in the first row (or grit (1, N)). Depending upon the configuration, these were the actual lengths that are swept by all rows present in the configuration and were the lengths for the descriptor estimation. (Fig.3-4).

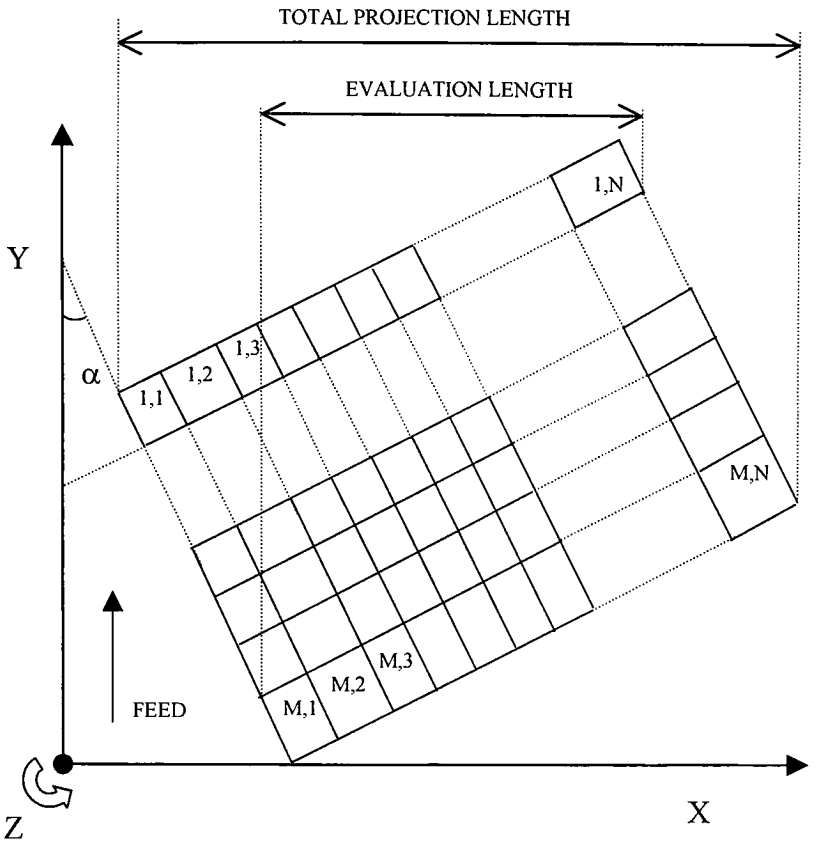

Fig 3-4: Total projection length and evaluation length.

The 3 dimensional tooling model is then projected onto two planes, the XY plane projecting the top view and the XZ plane projecting the side view of the tool. The projection of the tool in the XZ plane is done by translating the vertices of pyramid grits onto a plane with common Y coordinates (i.e. Y=0). The overlapping of pyramid grits along Y-axis creates a cumulative 2-D profile that resembles the multiple pass effect (Fig 3-5).

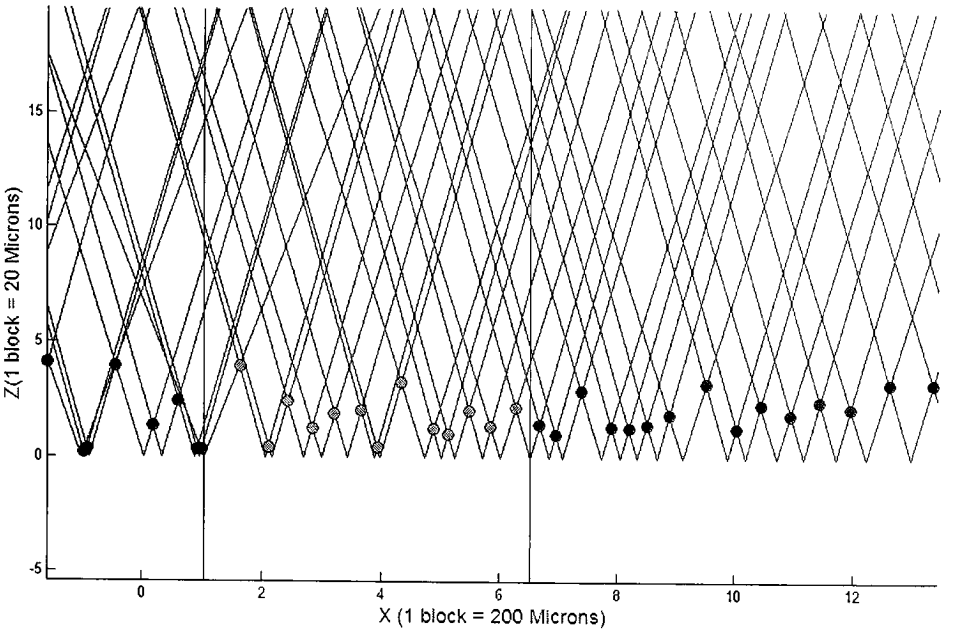

Fig 3-5: Multiple pass effect.

Thus the tooling model represents several aspects: from modeling the pyramid grit tool to the perspective view on the multiple pass effect at the specified attack angle.

3.2. Generation of workpiece surface

The next step after developing a tooling model was to represent the workpiece surface for the development of different surfaces before any machining has been performed. To understand the abrasive machining process, it was necessary to develop a workpiece surface whose descriptors were known. To develop a surface whose descriptors are known, a reverse metrology approach was followed. Figure 3-6 shows a flow chart of the surface generation process. The following surface descriptor: Average Roughness (R_a), Root Mean Square Roughness (R_q), maximum profile valley depth (R_v), maximum profile peak height (R_p), maximum peak to valley (R_t) as well as Skewness (R_{sk}) and Kurtosis (R_{ku}) were collected from an unmachined surface using both a stylus probe

profilometer and a light inferometer. From these surface descriptors, Root Mean Square Roughness (R_q) and Skewness (R_{sk}) were used as input for Gamma distribution. Figure 3-6 shows the flow chart of the generation of workpiece surface process.

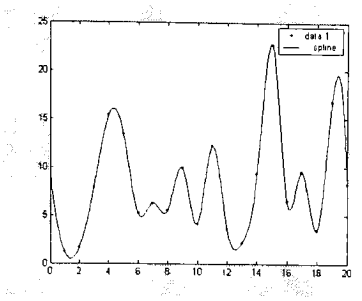

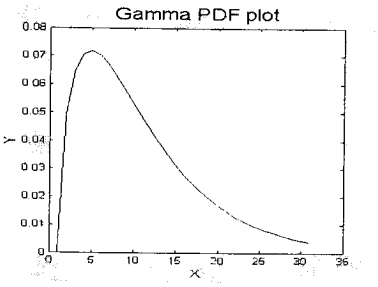

EXAMPLE:
R_q (stdv)= 8.4965,
R_{sk} (ske) = 0.6407.

Scan Surface

Measure Descriptors
R_a, R_q, R_{sk}, etc.

Fit Gamma Distribution

Generate Random Numbers

Fit a polynomial to develop the surface.

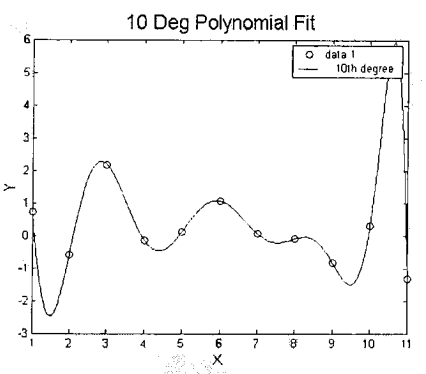

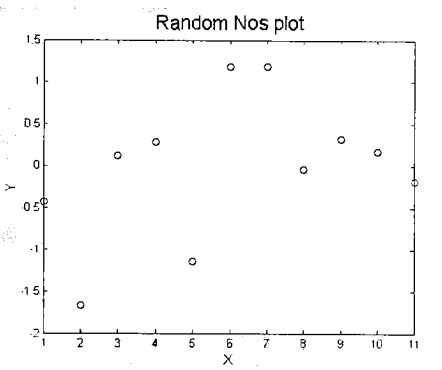

Fig 3-6: Flow chart of surface generation

As shown in Figure 3-6, Gamma distribution was used to generate a surface whose descriptors are known.

As described in section 2.3.4 the probability density function of gamma distribution is given by:

$$Y = \left(\frac{x}{b}\right)^{c-1} \frac{\left[\exp\frac{-x}{b}\right]}{b\Gamma(c)}$$

Where

b >0 is Scale parameter

c >0 is Shape parameter.

$0 < x < \infty$ is Range.

To determine the value of scale parameter (b) and shape parameter (c), the R_{sk}, S_{dv} values of an actual surface are used.

The Gamma distribution is generated in MATLAB as follows:

Gampdf(0:30,b,c)

Where,

(0:30) indicates the scale on X-axis

$$b = \frac{4}{R_{sk} * R_{sk}}$$

$$c = \frac{S_{dv}}{\sqrt{b}}$$

R_{sk} = Skewness

$$S_{dv} = \sqrt{\left[\frac{1}{N}\sum_{1}^{N}(x_i - \bar{x})^2\right]}$$

As a special case of S_{dv}, when $\bar{x} = 0$,

$$S_{dv} = \sqrt{\left[\frac{1}{N}\sum_{1}^{N}(x_i)^2\right]} \text{ Which is similar to } R_q = \sqrt{\left[\frac{1}{N}\sum_{1}^{N}(x_i)^2\right]}$$

Hence $S_{dv} = R_q$ (RMS Roughness)

Thus by using the roughness parameters of the original surface a gamma distribution is fitted. This creates a distribution from which it is possible to generate random points to fit many new random surfaces. These fitted surfaces will have, on the average, the same parameters as the distribution that originated the point and consequently will follow the parameters of the original workpiece surface.

This approach is suitable for a Monte Carlo simulation scenario. The random generation of surface allows for incorporation of variability into the workpiece surface while maintaining the average surface descriptors for each individual surface. 16 random numbers were generated from this Gamma distribution using the "gamrnd" function in MATLAB. To create a surface a 15 degree polynomial is fit through these points using another MATLAB function called "polyfit".

It was found that if the degree of the polynomial was increased beyond 20 degrees the polynomial oscillates and would not pass through all the points. The oscillations are due to a mathematical occurrence known as the *Runge Phenomenon.* It occurs due to the method in which polynomial interpolation is calculated and occurs when a large number of interpolation points are equidistant from each other. Due to this, the polynomial is ill – conditioned at the edges in the given interval. It is smooth in the center but oscillates at the edges. To deal with this oscillation phenomenon the concept of representative surface length was developed. (Fig.3-7).

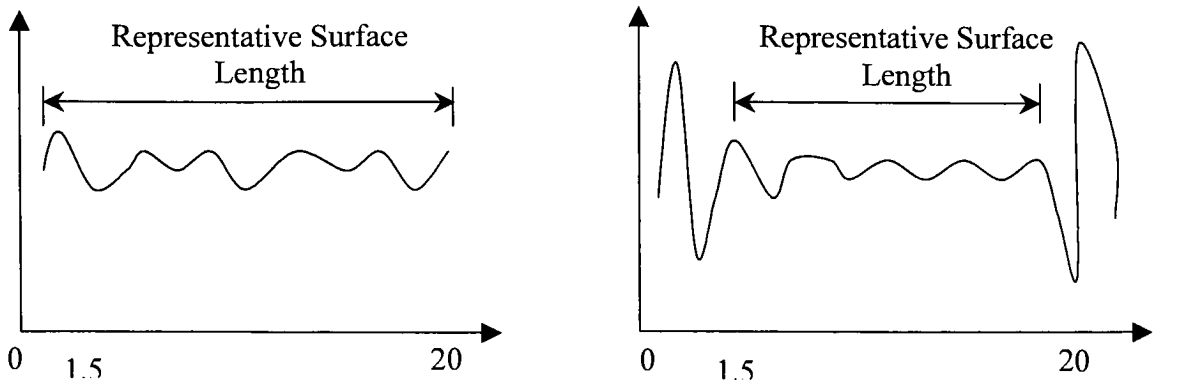

Runge Phenomenon Absent. **Runge-Phenomenon Present.**

Fig 3-7: Runge Phenomenon.

The representative section of the surface includes the smooth center section of the polynomial interpolation, while excluding the edges where the polynomial is ill conditioned. The remaining surface that includes the ill-conditioned polynomial is defined as the non-representative surface.

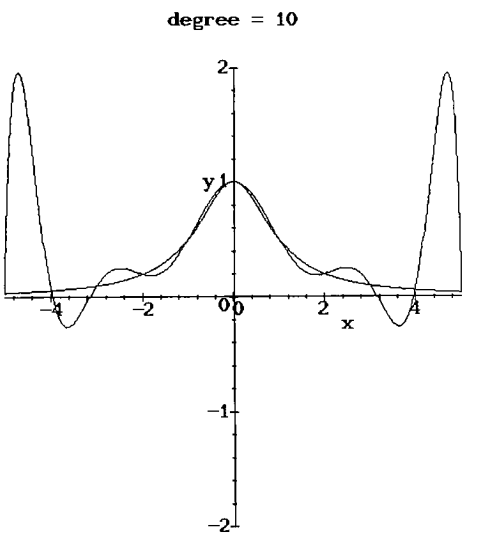

Fig 3-8: 10 deg polynomial interpolation in interval [+5, -5]

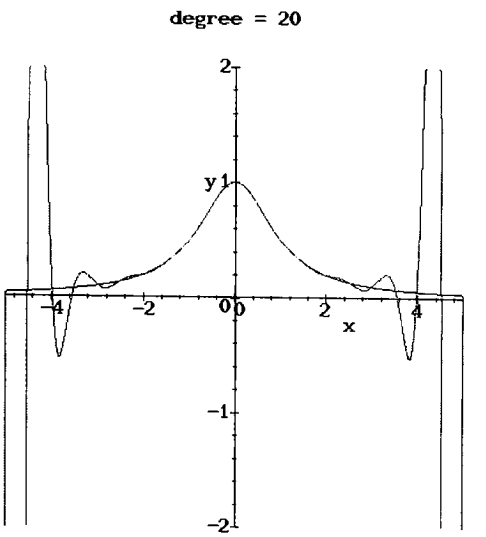

Fig 3-9: 20 deg polynomial interpolation for the same function in interval [+5, - 5]

Figures 3-8 and 3-9, demonstrate the Runge Phenomenon in polynomial interpolation. As can be seen the interpolation gets worse as the degree of polynomial is increased. In this work for generating the surface model, 15 degree polynomial was fitted as it provided a good range of random numbers while limiting oscillations at the extremities.

This Runge phenomenon can also be reduced to a certain extent by making the interpolation points closer to the edges instead of equidistant. The density of points at the boundaries of the interval is higher as compared to the center of the interpolation interval. This makes the polynomial smoother around the boundaries while the oscillations are reduced. This part is further discussed in detail in the future work section 7.

A 15 degree polynomial was determined to be the right degree for curve fitting using polynomials. The generated surface is then projected in XZ plane and superimposed with the 2D-pyramid grits tool projection (Fig 3-10). In this example a patch size of 2 X 2 is used to simulate the tool.

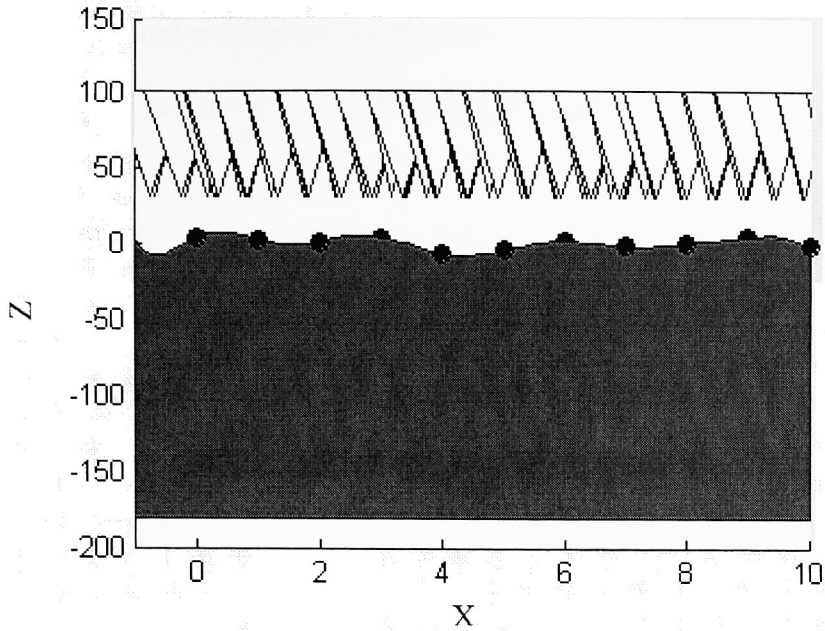

Fig 3-10: 2D surface and tool projection in XZ plane

Since the generated surface is 2D in XY plane, it is rotated around X-axis and projected into XZ plane. Homogeneous transformation matrix is again used to rotate the surface co-ordinates around X-axis.

The matrix used is:

$$T(\theta) = \begin{bmatrix} 1 & 0 & 0 & 0 \\ 0 & \cos\theta & -\sin\theta & 0 \\ 0 & \sin\theta & \cos\theta & 0 \\ 0 & 0 & 0 & 0 \end{bmatrix}$$

Where $\theta = 90°$

The workpiece and tool are now projected in the same plane and the interaction can now be modeled between the two to simulate the machining process. (Fig. 3-10)

3.3 Modeling of tool workpiece interaction

After developing the tooling and the workpiece surface models, the next step was to determine the interaction between the two. In order to calculate the surface descriptors of the machined surface it was necessary to determine the profile of the machined surface. Only after determining the point of intersection between the tool (pyramid grit) and the workpiece surface, can the machined surface profile be determined. The intersection points can only be calculated if the tool and surface are represented by some mathematical expression.

As previously shown the edges of the pyramid grits are represented by line equations and the surface by a polynomial equation. To obtain the points of intersection between the tool and surface, the two intersecting equations are solved simultaneously. The Newton Raphson Method is used to approximate the point of intersection between the line equations of tool and the polynomial equation of the surface. However, certain error was found in the approximation. A single pyramid grit is shown in figure 3-11 along with the surface that passes through the center of the grit. The point of intersection between the surface and the pyramid grit was approximated to be the center point. As seen in the figure there is an error in the X and Y coordinates calculated by the Newton Raphson method. Instead of the intersection point being calculated on the sides of the pyramid grits where the intersection takes place, it is calculated at its center. Figure 3-11 shows this approximation error in detail.

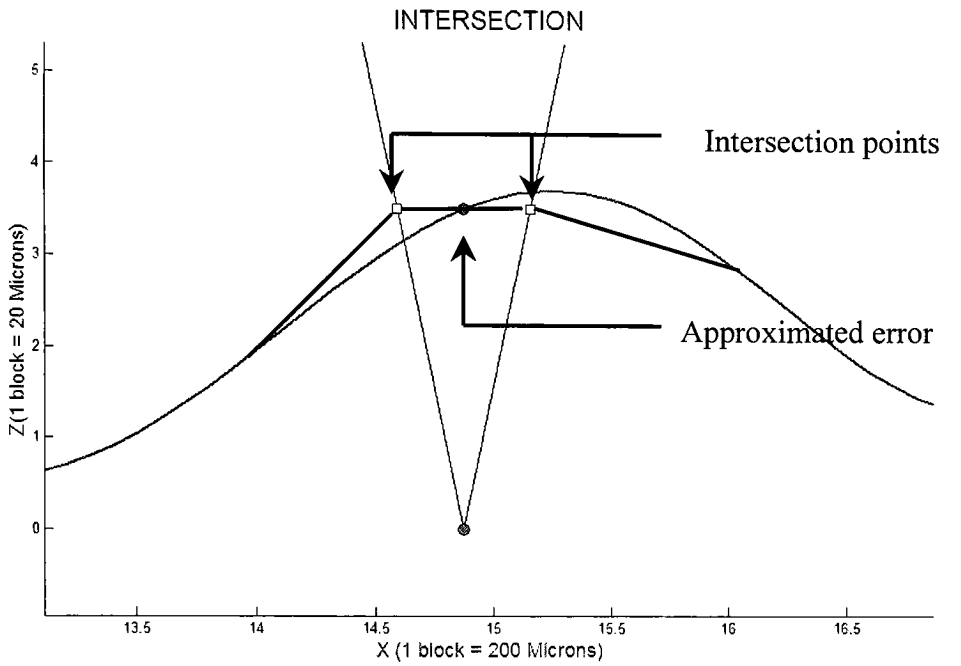

Fig 3-11: Approximation error and compensation.

To compensate for this error, the Y coordinate of this interaction point is substituted in the line equation (Y=mx + c), which represents the sides of the pyramid grits. The X coordinate of this interaction points is calculated as

$$X = \frac{y - c}{m}$$

Where y = substituted point.

c = constant

m= slope of the line.

These line equations are earlier calculated during parametric modeling of tool, (section 3-1). The new intersection points seen in Figure 3-11 falls on the side of the pyramid grit. Due to multiple points of contact between the tool and the surface, it is important to determine those points, which determine the final machined profile. An algorithm is

developed to screen the relevant points of intersection. The intersection occurs between the pyramid grits of the tool and between the tool and the workpiece surface (Fig 3-5). Only those points of intersection between the tool and the surface are relevant for determining the final machined profile. Only those points of interaction, which results in the workpiece surface being machined by the tool, considered being relevant. These points indicate the section at which the material is removed from the workpiece surface and indicate the profile of the machined surface. The developed algorithm screens these points. By connecting these screened points, the final machined profile is obtained (Fig 3-12).

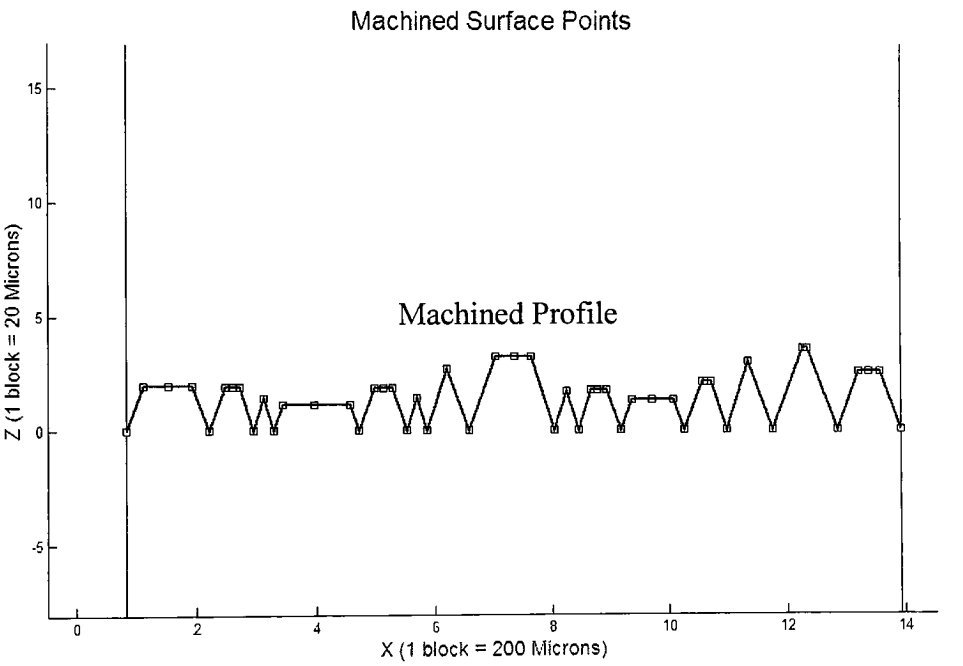

Fig 3-12: Machined Profile.

For ease of model validation, the assessment of roughness was performed to resemble a contact stylus profilometer. To calculate the surface descriptors the profile is scanned at a specific sampling rate. This sampling rate is calculated from the Mitutoyo SJ 401

profilometer which was used to calculate the surface descriptors of actual machined sample pieces. Under the settings of interest, this profilometer uses a sampling space of 0.05 microns. This sampling spacing of 0.05 microns is scaled into the program and used to develop the machine profile.

The program code developed, collects discrete number of data points and calculated the final surface descriptors, Average roughness (R_a), root mean square roughness (R_q), maximum profile valley depth (R_v), maximum profile peak height (R_p), maximum peak to valley (R_t) as well as skewness (R_{sk}) and kurtosis (R_{ku}). Refer to Appendix C for an explanation of such descriptors.

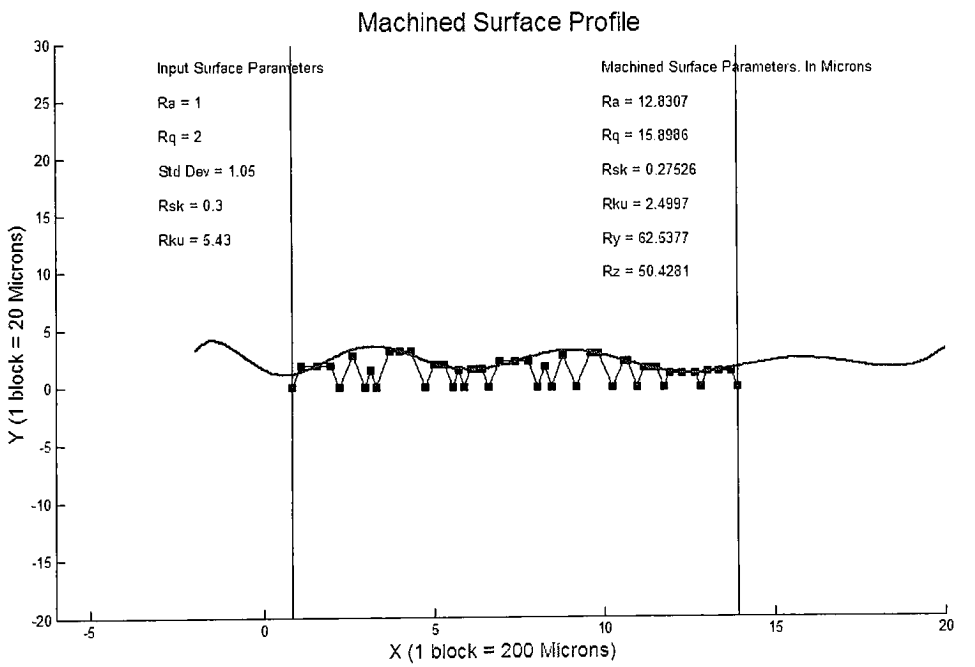

Fig 3-13: Resultant surface descriptors and profiles.

Figure 3-13 depicts the output from the program. It shows the calculated descriptors and the machined profile along with the original surface descriptor's and generated surface in the evaluation length. This figure gives details of the input parameters used to generate

workpiece surface and the resultant roughness parameters obtained from the machined profile. The details of the machined surface profile are also visible. Thus the machined surface profile is developed by the interaction between the tool and the work piece surface.

3.4 Graphical user interface (GUI)

There are 14 geometric parameters used as inputs to the program to develop the parametric tool (e.g. pyramid height, attack angle, etc), the workpiece surface (e.g. R_{sk}, R_q) and in the end to perform the interaction (e.g. indentation depth) between the two. There was a need for developing a front end for the program, so as to facilitate the entry of these 14 parameters without having to enter these parameters into the actual program code.

Hence the GUI (graphical user interface) was developed to allow the user to enter the required data in one stop easy entry format. Figure 3-14 shows a screen shot of this GUI for generating a tool with a patch size of 3X2 at 35°

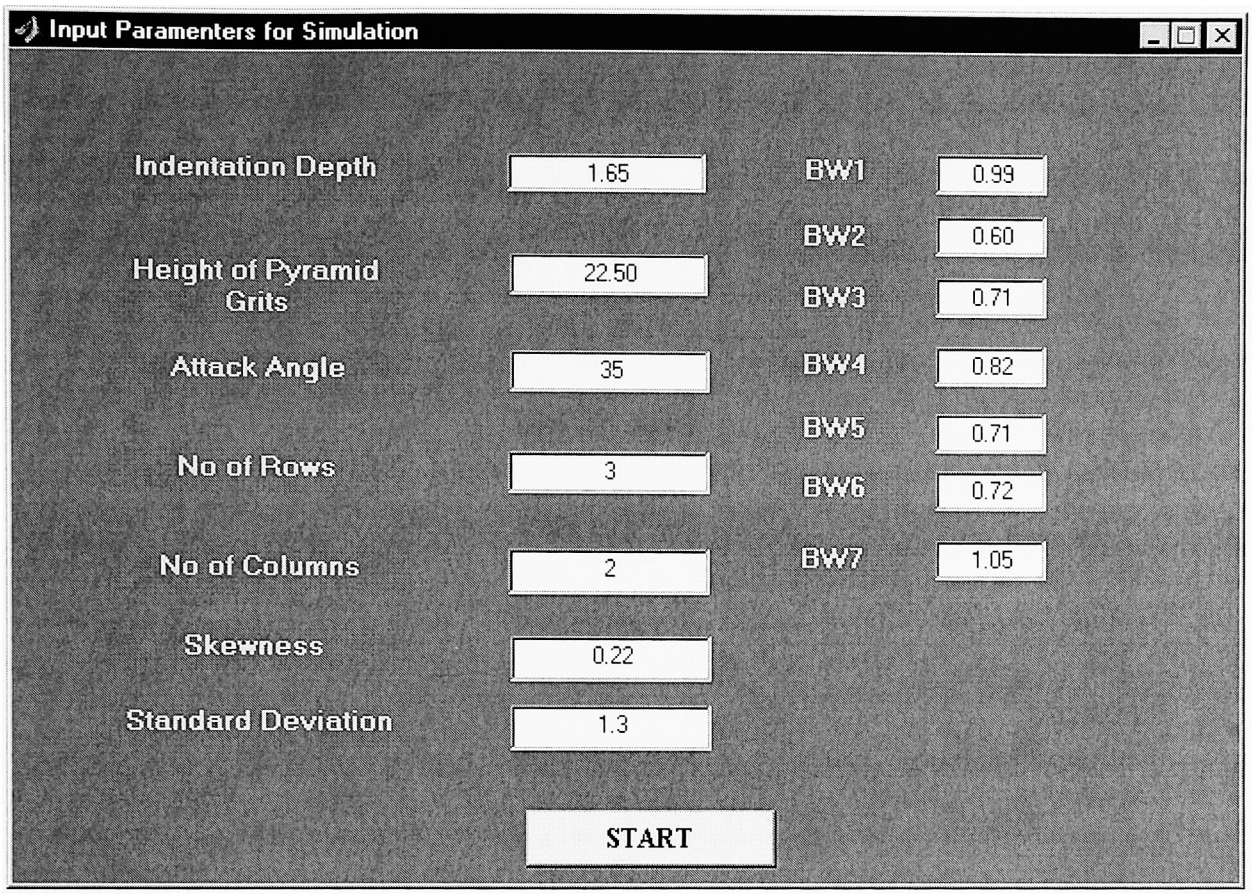

Fig 3-14: Graphical user interface (GUI)

Here, the required parameters for generating the tool, such as the height of the pyramid grits, and base widths are entered. BW1, BW2, BW3, BW4, BW5, BW6 and BW7 represent the 7 different bases that are used to make the seven different pyramids in a row. As mentioned in earlier section, a single patch consists of 7X4 pyramid grits. The aforementioned widths are used to form these 7 pyramid grits that compose one row. There are 4 such rows, which are constant and together form a patch. To generate the random workpiece surface the skewness (R_{sk}) and standard deviation (S_{dv}) of the original surface are required. These two descriptors are manually entered into the GUI as shown

in Figure 3-14. To perform the interaction between the generated tool and the workpiece surface, it is necessary to enter the indentation depth (how deep the tool penetrates below the surface mean line) and the attack angle (the angle at which the tool machines the surface).

Finally the tool size i.e. the number of rows and columns of patches of the pyramid grits to be used to machine the surface are entered. These determine the ultimate size of the tooling (i.e. length and width of belt). On entering all of these 14 parameters the program is ready to perform the algorithm. By clicking on the "start" button the program gets executed.

Since the program uses a certain scale to incorporate the actual values of the real surface and tool dimension, the data entered is scaled too. For e.g. The Z-axis for the tool uses the scale (1 unit = 20 microns). Hence to enter a height of the tool grit of 450 microns, a value of 22.5 is entered into the GUI.

The GUI allows the user the flexibility to modify the parameters as required in a very user-friendly environment and in the shortest possible time.

4. RESULTS

To calculate the results the program was run 10,000 times. To match experimental conditions, the configuration of the model was a patch size of (6 X 10), 34 μm indentation depth, base widths 1000, 630, 720, 830 and 740 microns in X-axis and 1000 and 720μm in Y-axis, 400 μm height and 0.05 μm scanning interval. To generate the random surfaces the surface descriptors are taken from two cases:

Case 1: Stylus profilometer instrumentation.

An unmachined mirror surface aluminum specimen is used and the surface descriptors calculated from the Mutitoyo SJ 400 profilometer with a 5μm stylus tip. The Root Mean Square Roughness (R_q) and Skewness (R_{sk}) are used as input to generate the random surface.

Case 2: Light Inferometer instrumentation.

The descriptors from the same unmachined mirror surface scanned by a Light Inferometer are used as input. (Light Inferometer uses laser beams to scan the surface and its smallest spot diameter allows it to penetrate into deeper cuts on the surface.)

The results of these iterations are shown in the table below.

Table 4-1 is divided into 2 major sections of results. The experimental value section refers to the surface descriptor values obtained from using surface profiling instruments such as the stylus profilometer and the light inferometer. The stylus profilometer uses a mechanical tip to scan the surface in the X and Z-axis. Hence it is referred to as 2D (2 dimensional) in the table. The light inferometer scans the surface using laser beams in X and Z-axis (2D) as well as in X, Y and Z-axis (3D). A mirror finish surface was scanned using both these instruments and the resulting values are used as input to generate the

workpiece surface in the computer model. Although the same mirror surface was scanned by the two instruments the results differ as different technologies are used for scanning. The laser beam is capable of reaching finer and deeper valleys in a surface than a mechanical tip and hence the surface seems less smooth in the case of light inferometer. The computer model section refers to the results obtained from the program developed in this work as well as an earlier model [9]. The results in the polished workpiece column were obtained when assuming a perfectly flat workpiece. The 10,000 iterations columns refer to the results obtained from this present work. The profilometer (2D) column shows the values obtained by using the profilometer readings as inputs. Whereas the light inferometer (3D) column shows results obtained when using the input from light inferometer reading.

Table 4-1: Comparative table between experimental and computer model results.

All values are R_a in microns.

	Experimental Values			**Computer Model values**		
Input	***Stylus Profilometer***	***Light Inferometer***		***Polished Workpiece***	***Profilometer (2D)***	***Light Inferometer (3D)***
	2D	**2D trace**	**3D**		**10,000 runs**	**10,000 runs**
Mirror finish Input	0.032		0.068		0.032	0.068
0° attack angle	***2.66***	***5.21***	***6.44***	***11.60***	***2.65***	***3.36***
35° attack angle	***2.45***	***4.79***	***4.47***	***6.10***	***3.39***	***3.38***

Table 4-2 shows the standard deviation and 95% confidence interval for the results obtained from the developed computer model. The 2D and 3D columns refer to the results obtained by using the profilometer and light inferometer respectively. The 0 deg and 35 deg are the attack angles used to machine the workpiece surface. As seen from the

above table 4-2, the low standard deviation indicates that the computer model provides consistent results. The 95% CI also shows very less variation in the results obtained by using this model. Thus the results from this work are comparable to the results from other instruments shown in table 4-1. Further analysis of these results is presented in the next section.

Table 4-2: 95% Confidence Interval of computer model results.

	2D			3D		
	95% CI		St. Dev	95% CI		St. Dev
0 Deg	2.54	2.75	0.18	2.67	2.67	1.19
35 Deg	3.29	3.48	0.02	3.28	3.48	0.05

5. ANALYSIS

As seen in table 4-1, in case of 2D, the results obtained from the computer model are comparable to those obtained from the Mutitoyo profilometer. For 0 degree attack angle the values are almost identical, which is an improvement from the earlier model, which had a very different result. When compared with the results from the inferometer there is 50% difference in the values but is still closer to the result as compared to the earlier model, which has a 145% difference in values. Thus the difference in result of this work is smaller as compared to earlier model. When compared, the values for 35 degree, the results are 50 % better than the polished workpiece model as compared with the results of the Profilometer. As compared to the results of the inferometer both the models show an equal amount of percentage discrepancy, around 30%.

In case of 3D, the results show a substantial increase in accuracy over the earlier model. The discrepancy is 47% as compared to 80% to the earlier model incase of 0 degree attack angle. For the 35 degree attack angle the discrepancy is 24.45% as compared to 36.31% of the earlier model [9] in the value of R_a descriptor.

The computer model mostly generates results that lie between the values given by the profilometer and the light inferometer. Hence the result indicates that the model is more accurate than the profilometer.

Thus it can be concluded that there is definite improvement in the accuracy of this model over the earlier ones. The surface roughness descriptors can now be predicted with better accuracy.

A possible explanation for the difference between the experimental and model values can be due to the fact that in actual machining the grits can undergo wear and fracture. The

grit geometry changes due to fracturing of tips during machining whereas, in the simulation model the grit geometry is assumed to be constant. No wear and tear is simulated. Due to this, the areas, which could have been left unmachined or lightly machined due to fracturing of tips or wear, are simulated to be completely machined in the model. Hence it finally results in the value of the surface descriptors being different.

Another reason for the difference could be due to the profile scanning technique. The profilometer uses a tip of certain diameter to scan the surface profile. The diameter of the tip limits the crevices in the valleys that the tip can measure (also called physical filtering). The light inferometer scans the surface, using laser and hence scans the machined profile better than the profilometer. Due to the very small diameter, the laser, can measure very tiny peaks and valleys and hence results in different descriptor values. The model uses line-scanning technique where the surface is evaluated at specific intervals and the values obtained are used to calculate the final machined profile. Hence the differences in measurement techniques result in different surface descriptor values.

Additionally, the dissimilarities in the values can be partially attributed to the material used. The actual material machined can create obstructions at times due to its chemical properties and lattice structure. Since the model considers only geometrical features, the influence of the chemical and physical properties of the wokpiece are assumed to be zero. This is not true in real life machining and hence results in variable descriptor values.

Finally, the fact that the material removal mechanisms are not 100% efficient also affects the final results. Earlier research carried out [22,34] found that approximately 15% of the groove volume is removed to form a chip, and that the remainder forms ridges on the metal surfaces. Also, the relative bluntness of non-ideally sharp tip decreases with

increasing penetration depth. The model assumes 100% material removal and infinitely sharp tip, thus leading to variance in final results

5.1 Noise matrix

To test the robustness of the model, noise was artificially introduced into the parameters. The program was then run to calculate the surface roughness descriptors. The geometric dimensions of the abrasive grits in the manufactured abrasive belts have some built-in variation. These could be due to any number of reasons in the manufacturing process. It was necessary to incorporate this variation in dimensions of pyramid grits and to analyze the effects of this variation in the final descriptor values. The analysis using a noise matrix addresses this issue.

To generate this artificial noise; the dimensions of the parameters were measured using the micrograph in the Sigma Scan software. A normal distribution was fitted for noise purpose and random numbers were generated using the average and standard deviation of these geometric dimensions. For example the height of the pyramid grits were measured 10 times and the average and standard deviation of these values was calculated. Using these values, random numbers were generated using normal distribution and the resulting values were used as noise in the noise matrix. Similar procedure was carried out for other parameters. A total of 256 runs were performed using this noise matrix and following results were obtained. See appendix A for more data on the noise matrix.

Table 5-1: Statistics of parameters used to develop Noise matrix.

(All values in microns)

	ID	PH	BW1x	BW2x	BW3x	BW4x	BW5x	BW1y	BW2y	Attack Angle	Skewness	Std Dev
AVG	34.10	455.07	1011.28	617.23	727.00	837.90	720.79	734.77	1084.84	34.83	0.10	0.02
STD DV	3.17	2.85	9.21	9.36	5.49	7.42	8.32	8.47	18.44	0.65	0.22	0.76
MIN	26.12	447.48	989.75	592.00	712.18	817.73	698.16	713.94	1039.46	33.19	-0.65	1.97
MAX	42.41	461.43	1035.10	639.94	740.33	856.09	741.19	757.21	1133.70	36.53	0.65	1.91

Table 5-2: Noise matrix result (all values in microns)

	Ra	Rq	Rsk
Mean	4.97	6.36	0.99
Standard Deviation	3.65	4.21	0.98
Maximum	22.86	28.18	2.62
Minimum	2.77	3.58	-3.36

As seen in Table 5-2 there is considerable difference in the minimum and maximum values. This is due to two reasons; one is due to a large standard deviation used to generate the random surface. Second reason for high roughness values is due to high amount of noise in the indentation depth. Table 5-1 indicates the statistics used to develop the noise matrix. From this table it is evident that the high degree of standard deviation in most of the parameters used to develop the matrix contributes to the high standard deviation in the results. The situations that contributed to the large variations in the mean occurred few times in the matrix, they influence the average, since these values are very high as compared to the normal average. These variations accorded only 9% of the entire 256 runs. Thus within the limitations of the variation in inputs

used to develop the matrix, the model provides consistent results. Since the variation in inputs is high, the variation in results obtained would be high too. Hence it is inconclusive at this stage whether the model is completely influenced by the noise.

5.2 Individual effect of parameters

To develop a better understanding of the effects of the individual parameters on the final roughness values, a main-effect (one factor at a time) analysis was carried out. The base settings for the factors were; pyramid height (415μm), number of grits per row (21), number of rows (20), sampling resolution (0.5μm), and depth of indentation (34μm). With only the exception of varying the factor of interest, these were the factor settings.

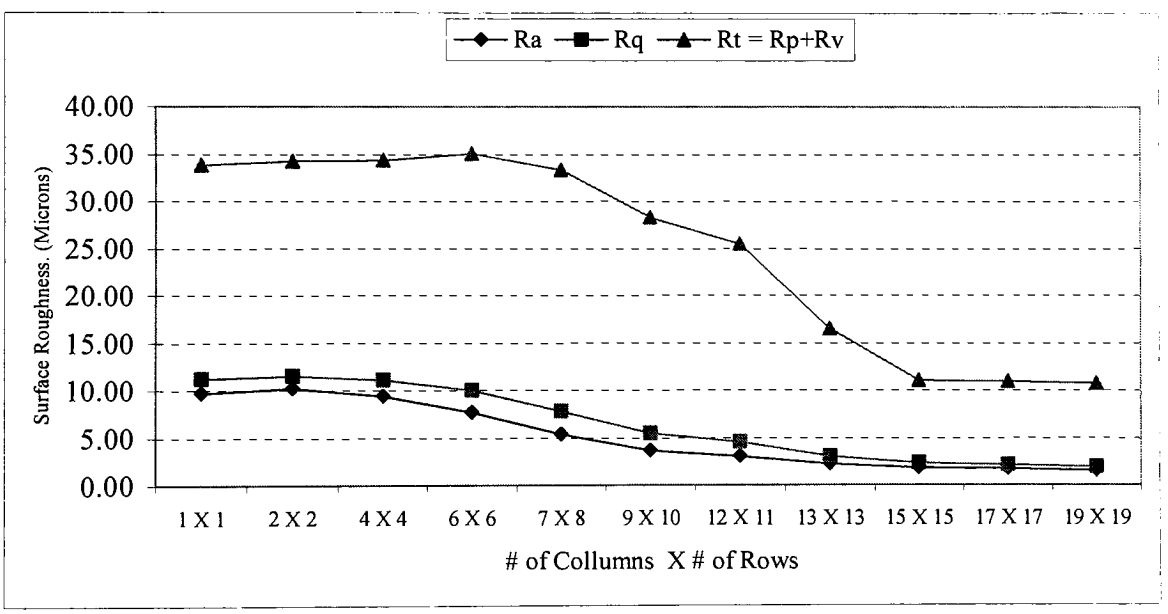

Fig 5-1 Individual effect of number of pyramids (number of grits per row and total number of rows).

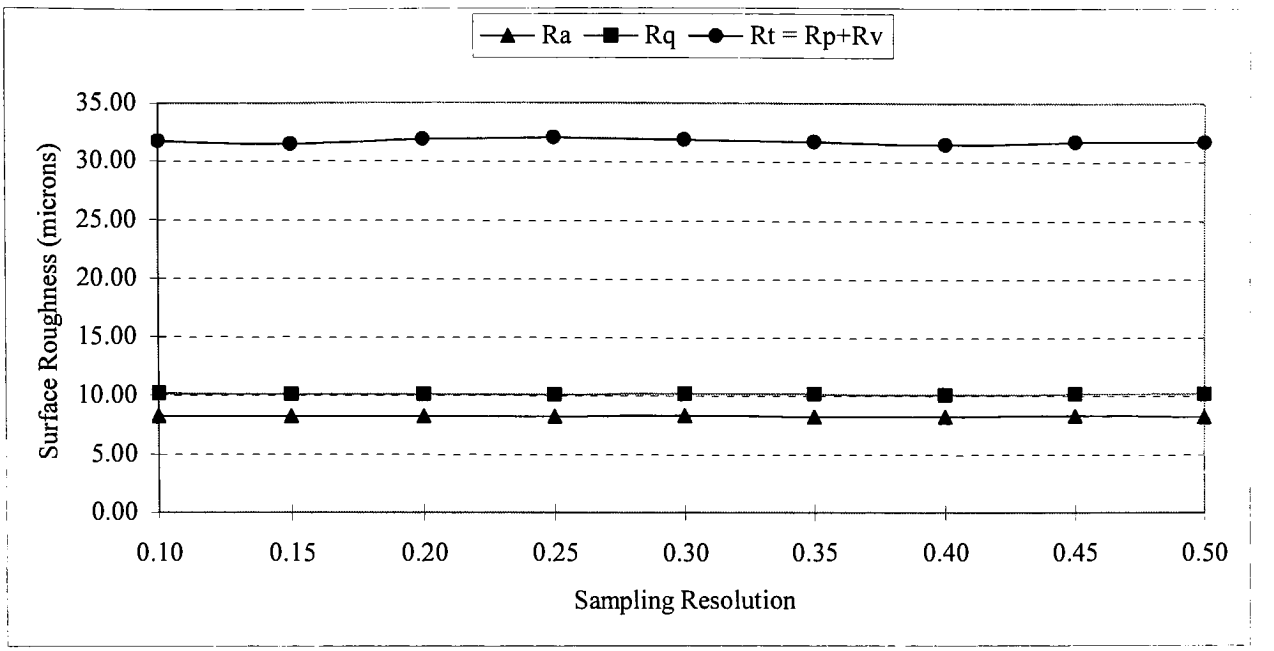

Fig 5-2 Individual effect of sampling resolution

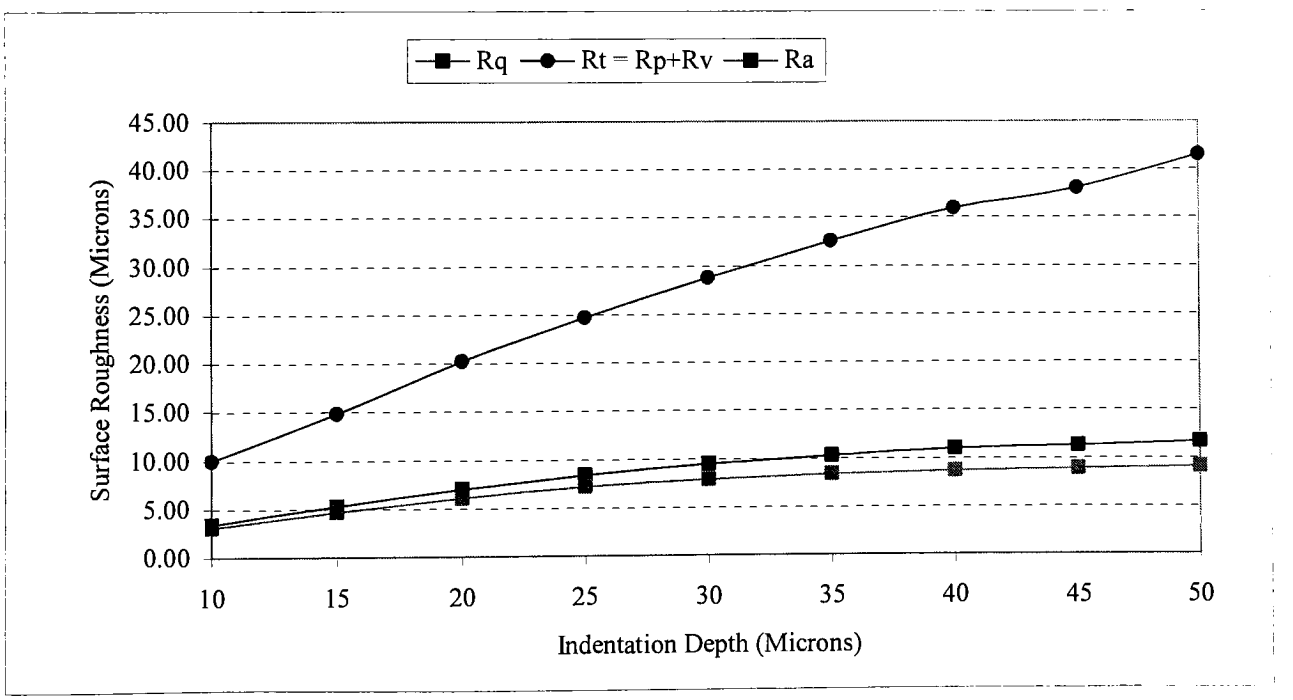

Fig 5-3: Individual effect of pressure applied (indentation depth)

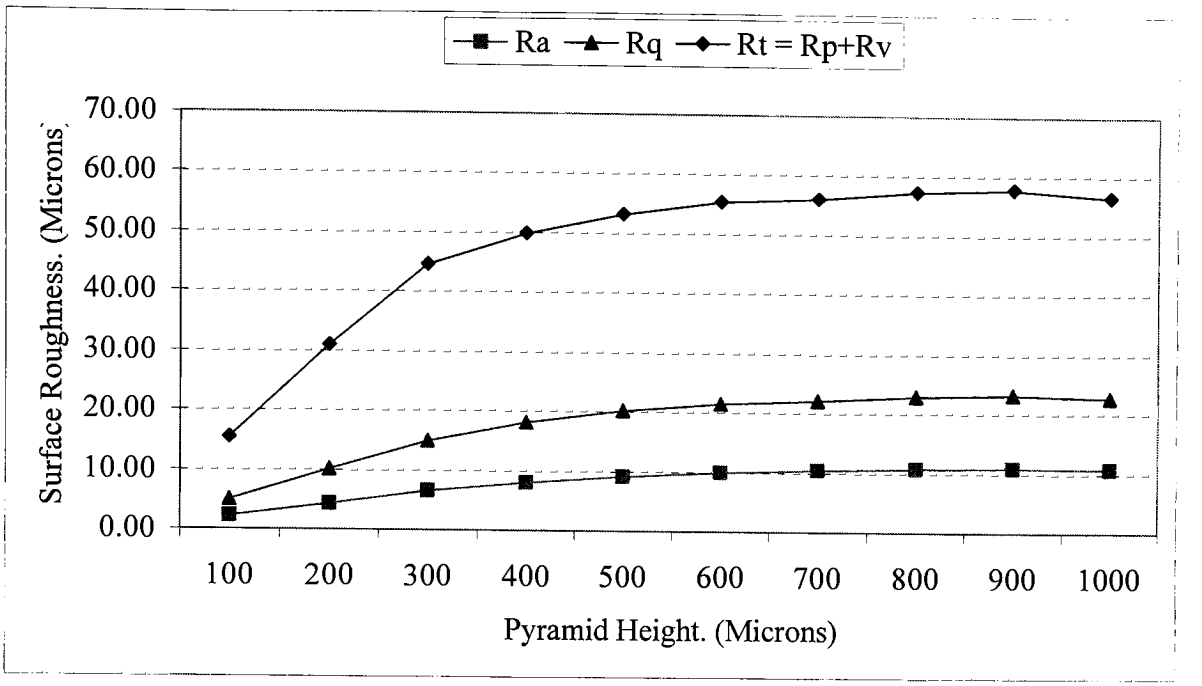

Fig 5-4: Individual effect of pyramid height.

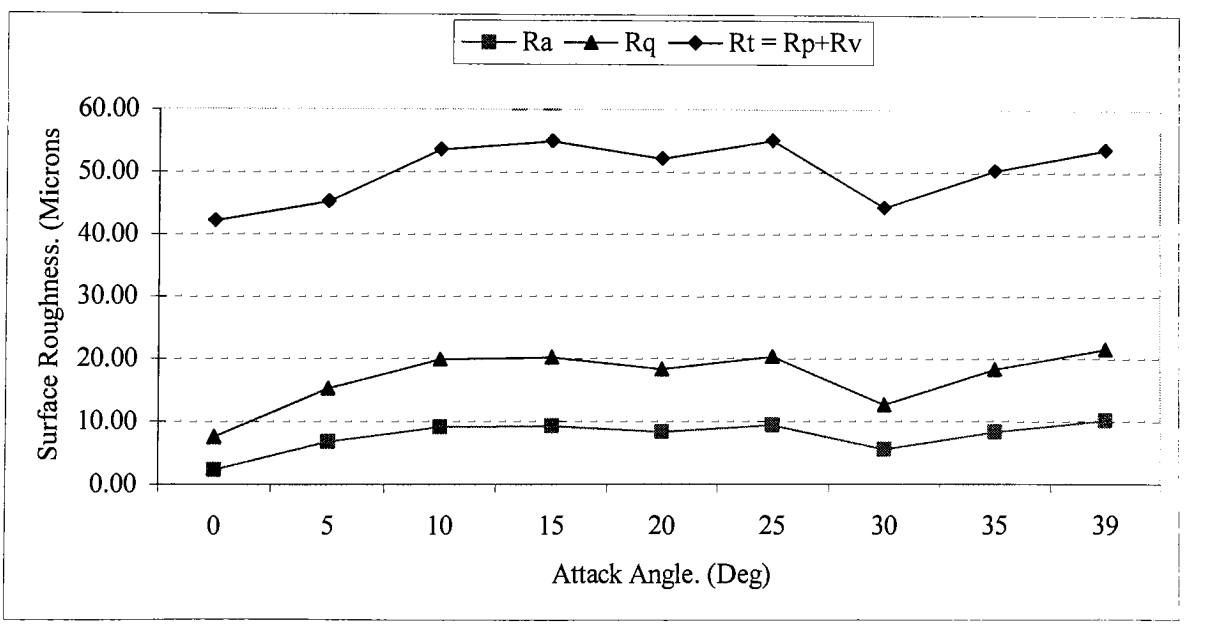

Fig 5-5: Individual effect of attack angle.

Figure 5-1 indicates that the number of pyramid grits does have a substantial influence on the surface roughness. The surface roughness descriptors R_a, R_q drop as much as 32 % for a 60% increase in the number of pyramids. However after a certain point the change is not that drastic and the descriptors approach an asymptote. Although there is change in the descriptors, it is not substantial enough to justify the increase in the number of pyramids. The decrease in value of roughness descriptors, indicating a smoother surface, is due to the multiple pass effect. As the numbers of pyramids are increased the number of grits interacting with the workpiece also increases and thus results in more material being removed. The section of workpiece left untouched by the front grit is removed by the next grit passing in the same line. But, as the numbers of grits keep increasing a point is reached when the following grits scratch at the same region where the grits before it have scratched. Thus the same area is machined again and again, leading to constant descriptor values.

As per Figure 5-2 there is no substantial evidence that increasing the scanning resolution affects the roughness descriptors. The R_t value shows some variation and this is because at higher scanning intervals the possibility of missing peak to valleys increases and thus results in variable descriptor values.

As seen in Figure 5-3 the indentation depth affects the value of descriptors R_t and R_q substantially. There is 78% change in the minimum and the maximum value of these descriptors. As the peaks and valleys increase with increase in indentation depth the value of R_t increases. At smaller indentation depth the tool barely scratches the surface. Hence a smoother surface is obtained. As the tool penetrates into the workpiece more material is removed and more peaks and valleys created as the depth

increases. This occurs only up to a certain depth after which the values become constant.

Figure 5-4 indicates that as the pyramid height increases the roughness of the machined surface also increases. Although there is substantial increase, around 352% in the surface descriptors as the pyramid height is changed from 100 to 400 microns, the change is hardly 5% above 500 microns height. Shorter pyramid with larger base removes more material than taller grit with smaller base. Since the indentation depth is constant, and the height increases, the area of the tool coming in contact with the workpiece decreases. As the pyramid height increases, lesser amount of surface comes in contact with the tool, leading to an increase in the peaks and valleys. As the number of peak and valleys increases the roughness of the machined surface increases until it reaches a point where the difference is negligible. After a point the change in affect of the change in height is insignificant.

Figure 5-5 suggests that the angle of attack at 0 degree gives the best surface as compared to other angles. However, due to the geometric dimensions of the pyramid base grits and the 0 degree angle only 5 pyramid grits interact with the surface to form the new machined surface. Since the input surface parameters have very small roughness, the value of the new machined surface is influenced by these values, leading to an impression that the 0 degree attack angle gives the best surface.

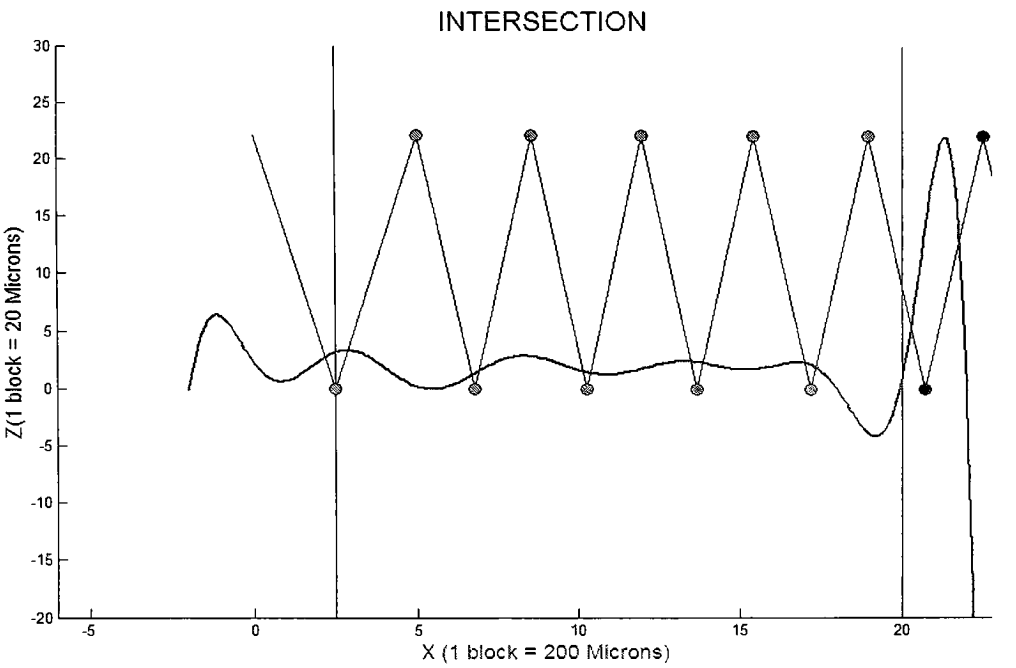

Fig 5-6: 2D view of the tool and work piece interaction at 0 deg attack angle.

Figure 5-6 above shows the interaction between the tool at 0 degree attack angle and the workpiece. As mentioned there is minimum interaction at this angle. This is due to the fact that at 0 degree the pyramid grits line up behind each other. And hence only 5 grits in the 2D plot are seen instead of 20 rows and 21 grits/row (11760 grits), which make up the tool in this case.

Since the workpiece surface here is a highly polished surface, the final profile obtained represents the workpiece surface with few indentations made by the tool. Hence the 0 degree attack angle results in a very smooth surface.

If the 0 degree attack angle is neglected then according to Figure 5-5, the 30 degree angle gives the best surface. As the attack angle increases from 0 degree to 30 degree the surface roughness increases and at 30 degree the best surface is obtained. As the angle is further increased the roughness again increases, leading to the conclusion that

the 30-degree attack angle is the best surface yielding attack angle. The R_q value obtained at 30 degree is 38 % better than the worst case at 39 degree. Earlier research [9] has shown that 35 degree attack angle is the best, but current research shows that the value of R_a and R_q descriptors obtained at 30 degree is 29.47 % better than those at 35 degree.

The various conclusions that can be drawn from this analysis are presented in the next section.

6. CONCLUSION

Until now there was no accurate model to simulate or analyze the actual abrasive machining process with multiple-pass effect. This parametric model represents a tool that can be used for such purposes. The analysis carried out proves the robustness and accuracy of this model. It also incorporates the multiple pass effects that hitherto were not analyzed by other models [46]. It can be concluded that a model to calculate the effects of various geometric parameters on the workpiece surface is available.

The flexibility to accept input through a graphical user interface (GUI) for parameters such as base widths, pyramid height, the number of pyramids, attack angle, sampling resolution, and the indentation depth, surface roughness parameters to generate the random surface is the most important feature of this model. The GUI makes the model simple and easier to use.

The tooling model is highly flexible, allowing the researcher to manipulate various geometric features (pyramid height, base, etc). The ability to manipulate the number of abrasive grits allows for further analysis into intricate machining processes of abrasive grinding. The ability to use attack angle at any degree gave the opportunity to determine the best possible attack angle. It also put forth the effects of different attack angles on the roughness of the machined surface. It provides an excellent opportunity for a better understanding of the behavior of the pyramid grits at different angles. It also allows the opportunity to study the multiple pass effect on the work piece surface. Due to the multiple pass effect, the abrasive grits cut through the work piece one after the other and increase the amount of material removed, thus increasing the material removal rate. This phenomenon could not be analyzed in earlier models,

which used just single grit. Due to the multiple grits that can be specified in the program, effects of the number of grits can be analyzed. Statistical verification carried out on the results of the model, provides robust analysis of their performance.

Another, big advantage of this model is the ability to generate random surfaces whose surface roughness is known. The technique of generating random numbers using Monte Carlo method incorporates the variability that occurs in nature. Surfaces having different shapes but similar roughness descriptors occur in nature. Generating random surfaces having similar roughness descriptors has been the most challenging part in this model. It provides a unique set of problems. Successfully simulating these random surfaces not only makes the model highly robust but also increases its efficiency and accuracy. It also brings the model a step closer to the real life scenarios.

Polynomials are one of the simplest curves found. The use of polynomial curves to represent the workpiece surface makes it a simpler mathematical problem to calculate the surface descriptors as compared to the use of other curves such as Bezier or B-Spline curves. It is very simple to calculate the value of the surface at any point in the interval. Hence when evaluating the machined profile, scanning the polynomial surface becomes very simple and easy. Hence the calculation of the final machined profile becomes a simple matter of substitution into their respective mathematical equations.

The extensive analysis carried out with the model leads us to the following conclusions about the various geometric parameters in the model.

- As mentioned earlier, the multiple pass effect significantly influences the roughness of the machined surface. As the number of pyramid grits increase the roughness of the machined surface reduces (i.e.) a smoother or more polished surface is obtained. After a certain point though, any increase in the number of pyramid grits fails to affect the roughness values in a significant way. This indicates that the optimized level was reached. The model indicates that 13 grits/row and 13 rows (4732) of pyramids is the optimized level. This would serve as a valuable reference to the manufacturers of engineered abrasives.
- Increasing the sampling resolution from 0.1 micron to 0.5 micron show no significant difference in the roughness descriptors in that interval. Thus any instrument having scanning interval between this range, can be used to measure the surface descriptors. Hence an instrument having a scanning interval of 0.5 microns can be used as compared to a more expensive 0.1-micron resolution instrument.
- The individual effect of indentation depth indicates that the deeper the tool penetrates into the workpiece, the higher the roughness value of the machined surface. This indicates that the deeper the tool penetrates into the surface the higher the number of peaks and valleys created during machining, thus resulting in increased roughness of the machined profile. Hence digging deeper into the workpiece results in more material removed but not necessarily results in a smoother surface.

- The individual effect of pyramid height shows an initial increase in roughness descriptors followed by a constant trend. A smoother surface is observed with smaller pyramid height and as the height increases the roughness too increases. This is obvious since for a constant base width a shorter pyramid height results in a short tool having a broader surface area in contact with the workpiece will result in much smoother surface than a taller tool with lesser surface area. This would seem natural as the pyramid indentation depth is fixed to a certain level. Since the tip penetrates the surface the increase in height affects the roughness initially and its effect remains unchanged beyond a certain height.
- Due to the ability of the model to incorporate various attack angles, it was observed that a 30 degree attack angle results in the smoothest machined surface.

The values obtained were compared against earlier experiments and validated. The model represents an efficient and accurate analysis tool as compared to earlier attempts. The trends and values are close to the actual experimental values. Hence this parametric model simulates the abrasive machining process and also suggests, the geometric parameters to obtain the optimal surface finish from a workpiece.

7. FUTURE WORK

Future work can be carried out in two areas of this model; one would be to increase the efficiency and accuracy of this model and second to make the model more general by incorporating other engineering abrasive shapes.

To increase the accuracy of this model a larger surface area can be used than the one used in this model. Since the degree of polynomials restricts the number of random number generated which in turn restricts the length of the surface, multiple polynomials can be used to connect to each other and hence increase the length of the surface. For e.g. two 16 degree polynomials can be used to form one surface. Hence a higher number of pyramids with various base widths can be used to calculate the surface roughness. This would increase the accuracy and robustness of the model.

Polynomials are the simplest curves. They have simple mathematical equation describing them and it is very easy to calculate the value of a polynomial at any point. But there are various curves such as Spline, B-Spline, Bezier Etc curves that can be used to represent the surface. It would definitely be a step forward to see how the model performs and what results are obtained when different curves are used to represent the surface.

In this model the pyramid has an infinitively sharp tip at its bottom. In real life as the abrasives are machined, the edges become smooth due to wear and tear. To incorporate this change the edges can be represented by a smooth arc or semicircle. This would make the model more realistic and the results would be more comparable to the actual machining results. But it should also be noted that the model would be more complicated.

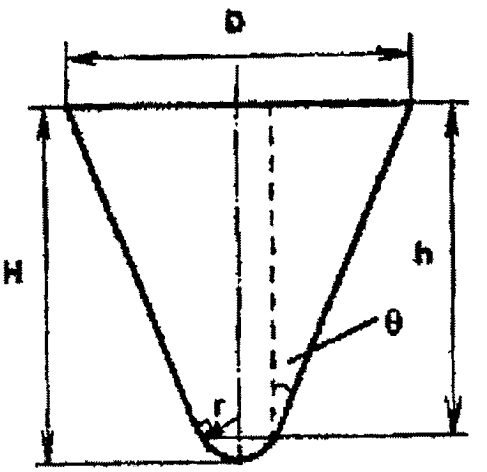

Fig 7-1: Pyramid grit with round tip. (Source [36])

Figure 7-1 shows conical shaped grit with round tips. This figure is taken from a paper by Liang Fang [36]. In this work a simulation of single tip abrasion is performed and analysis carried out. This conical shaped grit can be used as reference to generate smooth curved pyramid grits as a continuation of present work. The dimensions for this grit are given by:

$$D - 2r\cos\theta = 2h\tan\theta$$

$$H = h + r(1 - \sin\theta)$$

Where h – height of grit frustum.

D – grit diameter.

H – grit height.

r – tip radius.

θ - apex angle

There are only three independent variables. Therefore, D and H were assumed to follow Gaussian normal distribution. The tip radius *r* was assumed to have a uniform distribution. The distribution of the apex angle θ and the frustum height *h* are dependent

upon other variables and their distribution as shown by equations above. These equations could be useful in developing a future model with conical shaped pyramid grits.

Future work in developing the workpiece surface can be carried out in the area of curve fitting. As explained earlier, an undesirable effect of using polynomials for curve fitting is the Runge Phenomenon. The oscillations at both the edges of the polynomial curve fit result in an ill-conditioned surface. This is due to *equidistant interpolation with polynomials of high degree.* To over come this problem, **Tchebycheff abscissae**, can be used. Since the cause of oscillations is due to the equidistant points, it is necessary that the points be scattered. Tchebycheff abscissae, reduces the distance between the points at the outside of the interpolation interval and the distance between points in the center is increased by a small value. Since the distance between the points at the outside of the interval is reduced, the polynomial is *well conditioned* in the interval of interest.

In general, Tchebycheff abscissae is given by:

$$x_i = \cos\frac{2i+1}{m+1}\frac{\pi}{2}, \qquad \text{i} = 0,1,2,\ldots\ldots\ldots,\text{m}, \quad (\text{m} = 10)$$

To demonstrate this solution, 11 random numbers were generated and a 10 degree polynomial was used to fit the data in the interval [-1,1].

Figures 7-2 and 7-3 show the 10 degree polynomial curve fit before and after using Tchebycheff abscissae.

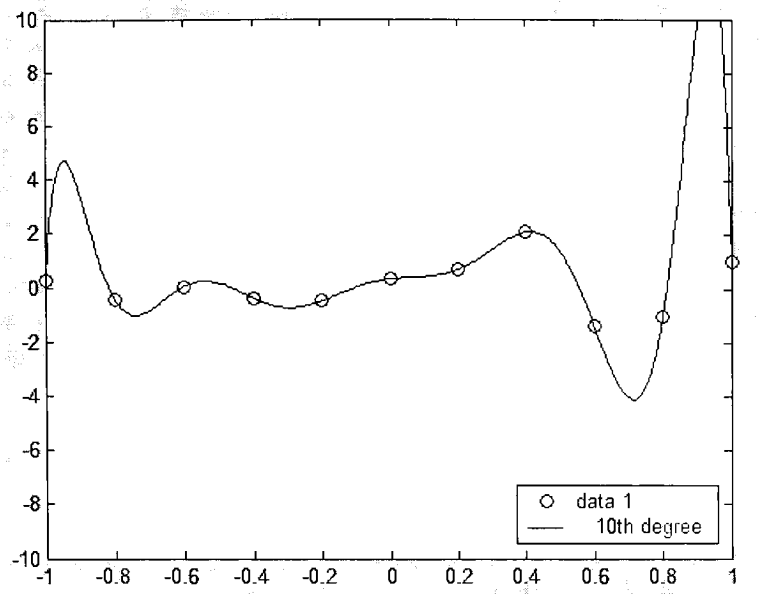

Fig 7-2: 10^{th} degree polynomial fit before using Tchebycheff abscissae.

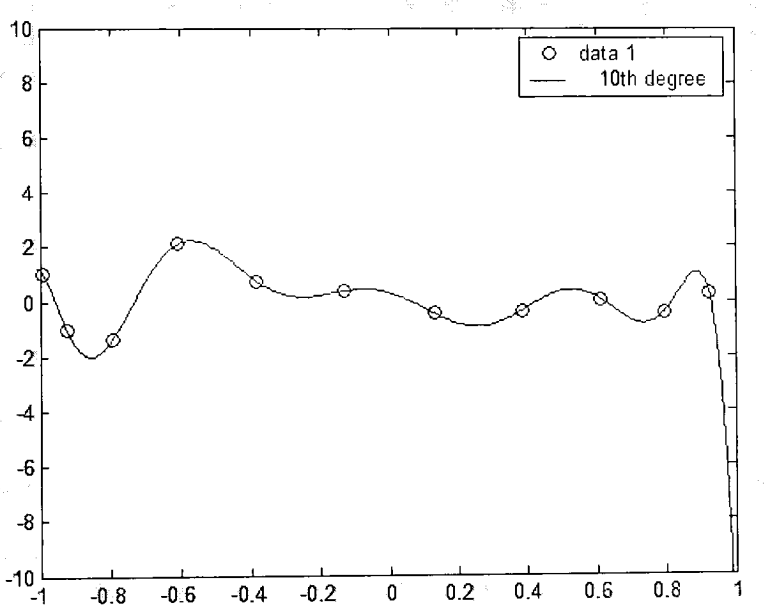

Fig 7-3: 10^{th} degree polynomial fit after using Tchebycheff abscissae.

As seen from the above figures, the Tchebycheff abscissae is successful in reducing the effects of Runge Phenomenon. This new surface can be used as a workpiece surface in future models. The conclusion drawn from this work as regards to abrasive geometry in section 6 can be used as basis for further studies into application specific engineered abrasives. Example, for developing smooth surface, pyramid shaped grits with small height and large base are recommended. Experiments can be carried out using such engineered abrasives on different metal and wood surfaces to further verify results.

Different geometries can be introduced and developed to further strengthen this model. Quad and helical shaped abrasives can be similarly modeled and the results obtained would give an interesting perspective on how different abrasive geometries affect the final roughness of the workpiece.

8. REFERENCES

1. ASME B46.1 (1995). Surface Texture (Surface Roughness, Waviness, and Lay). An American National Standard. The mechanical Society Of Mechanical Engineers. New York, New York.

2. Bly. W. R, Blake. G. (1982). Technical Writing, Structure, Standards, and Style. McGraw-Hill. New York, New York.

3. Brown, C. A., Savary. G. (1991). Describing ground surface texture using contact profilometry and fractal analysis. Wear. Vol. 141. pp. 211-226.

4. Boothroyd, G., Knight, W.A. (1989). Fundamentals of Machining and Machine Tools. Second Edition. Marcel Dekker, Inc. New York.

5. Buslenko .N. P, Golenko. D .I, Shreider. Yu. A, Sobol I. M, Sragovich .V. G. (1966). The Monte Carlo Method, The method of statistics trials. First edition Pergamon Press Ltd. Oxford/ London.

6. Buttery, T.C., Hamed, M.S. (1997). Some factors affecting the efficiency of individual grits in simulated grinding experiments. Wear. pp. 231-245.

7. Carr Lane Manufacturing Co. (1991). Modular Fixturing Handbook. Second Edition. Edited by Carr Lane Mfg. Co. St. Louis. Missouri.

8. Carrano, A.L. (1997). Quantification of the effect of process parameters and their interactions with respect to material removal rate and surface roughness for a wood sanding process in the furniture making industry. Master Thesis. Department of industrial engineering. North Carolina state university. Raleigh, North Carolina.

9. Carrano, A.L. (2000). Characterization of wood surface preparation. Ph.D. Dissertation. Department of Industrial Engineering. North Carolina State University. Raleigh, North Carolina.

10. Cheng, C.S, Jacroux, M. (1998). The construction of trend-free run orders of two-level factorial designs. J. of the American Statistical Association. Theory and Methods. December. Vol 83. No. 104.

11. Dean, A., Voss, D. (1999). Design and Analysis of Experiments. Springer-Verlag. New York, New York.

12. Dornfeld, D.A. (1981). Single-grit simulation of the abrasive machining of wood. ASME/ Journal of Eng. For Industry. Vol. 103:1-12 New York.

13. Edvarsen, K. (1993). A method to study the quality of planed surfaces and its influence on glue-line strength. Proceedings of the 11th International Wood Machining Seminar. pp 496-497

14. Evans. M, Hastings. N, Peacock. B. (1993). Statistical Distributions. Second edition. John Wiley & Sons. New York, New York.

15. Fargo, F.T., (1982). Handbook of Dimensional Measurement. Second edition. Industrial Press Inc, New York, New York.

16. Fisher, R. (1993). Principles of surface formation. Proceedings of the International Conference on Woodworking Technologies. Hannover. Germany.

17. Franz, N.C., Patronsky, L.A. (1954). Machining wood with coated abrasives. University of Michigan Project Report#1, project Number 2082.

18. Gahlin, R., Jacobson, S. (1996). The effects of compressive stresses on the abrasion of diamond coatings. Wear. Vol 196. pp- 226-223.

19. Gahlin, R., Jacobson, S. (1997). Micromechanical manufacturing of abrasive surfaces for fundamental studies in wear and grinding. Wear. Vol 217. pp- 231-236.

20. Gahlin, R., Jacobson, S. (1998). A novel method to map and quantify wear on a micro scale. Wear. Vol 222. pp- 93-102.

21. Gahlin, R., Jacobson, S. (1998). The influence of tip shape in abrasion studied by controlled multiasperity surfaces. Wear. Vol 223. pp- 150-156.

22. Gahlin, R., Jacobson, S. (1999). The particle size effecting abrasion studied by controlled abrasive surfaces. Wear. Vol 224. pp- 118-125.

23. Gerald F. (2002). Curves and Surfaces for CAGD, A practical guide. Fifth edition. Academic Press. San Diego, California.

24. Goldstein, J.I., Newbury, D.e., Echlin, P., Joy, D.C, Romig, A. d., Layman, C.E., Fori, C., Lifshin, E. (1992). Scanning Electron Microscopy and X-Ray Microanalysis. Second edition. Plenum Press. New York. New York.

25. Groover M. Fundamentals of Modern Manufacturing. Second edition.Prentice hall, Englewood cliffs, New Jersey.

26. Hammersley. M. J, Handscomb. D. C. (1964). Monte Carlo Methods. John Wiley & Sons. New York, New York.

27. Hicks, C.R., Turner, K. V. (1999). Fundamentals Concepts in the Design of Experiments. Fifth edition. Oxford University Press. New York, New York

28. Jiaren J, Fanghui S. (1998). Modelling of two-body abrasive wear under multiple contact conditions. Wear 217. pp 35-45.

29. Komanduri. R. (1971). Some aspects of machining with negative rake tools simulating grinding. Int. J. Mach. Tools Des. Res. Vol.11, pp 223-233.

30. Komanduri. R., Shaw, M.C. (1977). Scanning electron microscopy study of surface characteristics of abrasive materials. Journal of Engineering Materials and Technology. July. pp 145-156.

31. Kuehl, R.O. (2000). Design of Experiments: Statistical principles of research design and analysis. Second edition. Pacific Grove. Duxbury-Thompson learning.

32. Lafara. L. R. (1973). Computer Methods for Science and Engineering. Hayden Book Company. Rochelle park, New Jersey.

33. Lancaster. P, Salkauskas. K. (1986). Curve and Surface Fitting, An introduction. Academic Press. Sandiego, California.

34. Larsen-Badse, J. (1968). Influence of grit diameter and specimen size on wear during sliding abrasion. Wear. 12, pp 35-53.

35. Lemaster, R. L., Dornfeld, D. A. (1963). The use of acoustic emission to monitor an abrasive machining process. 11th International Wood Machining Seminar. Norway.

36. Liang F, Jiandong X (2001). Computer simulation of two-body abrasion process. Wear 251, pp 1356-1360.

37. Maron. J. M. (1982). Numerical Analysis, A practical approach. Macmillan Publishing. New York, New York.

38. Mulhearn, T. O., Samuels, L.E. (1962). The abrasion of metals: a model of the process. Wear. Vol 5. pp. 478-498.

39. Ned A. (1974). Numerical Methods. Prentice-Hall, New Jersey.

40. Nielsen. L. K. (1965). Methods in Numerical Analysis. Second edition. The MacMillan Company. New York, New York.

41. Norton Co. (2000). Coated abrasives' 3-D structures yield higher efficiency and longer life. Modern Applications News. April.

42. Oxley, P.L.B. (1997). Modeling the related processes of abrasion, wear, and polishing. Advances in Abrasive Technology. L.C. Zhang and N. Yasunaga Editors. World Scientific. Sydney, Australia.

43. Pfestorf, M., Engel, V., Geiger, M. (1998). 3D- Surface Parameters and their application on deterministic textured metal sheets. International Journal of machine Tools Manufacturing. Vol 28 (5-6). pp. 607-614.

44. Rogers. F. D. (2001). An Introduction to NURBS, with historical perspective. Academic Press, California.

45. Samuels, L. S. (1971). Metallographic Polishing by Mechanical Methods. Second Edition. American Elsevier Publishing Company, Inc. New York, New York.

46. Samuels, L. S. (1978). The mechanics of abrasive machining. Scientific American. November. Vol 239(5). pp. 132-152.

47. Schmidt, S. R., Launsby, R. G. (1994). Understanding Industrial Designed Experiments. Fourth Edition. Air Academy Press. Colorado.

48. Sedricks A.J, Mulhearn, T.O. (1963) Mechanics of cutting and rubbing in simulated Abrasive Process. Wear. Vol. 6, issue 6, pp 457-466.

49. Shaw, M.C. (1996). Principle of Abrasive Processes. Oxford Series on Advance Manufacturing. Oxford University Press, Inc. New York, New York.

50. Sin, H., Saka, N, Suh, P. (1979). Abrasive wear mechanisms and the grit size effect. Wear. Vol 55. pp. 163-190.

51. Smulski, S. (1980). A close look: micrographs illuminate sanding, scraping and planning. Fine Woodworking. March/April.

52. Sobol. M. I. (1974). The Monte Carlo Method. The University of Chicago Press. Chicago, Illinois.

53. Stewart, H. A., (1978). Stock removal rate for aluminum oxide and garnet coated abrasive belts. Forest Prod. J. Vol.28.

54. Story, R. H. (1979). Estimating of HP requirements for belt grinding operations. Proceedings of the Sixteen Annual Abrasive Engineering Society Conference. Pittsburgh, PA. May 14-16.

55. Taylor, J. B., Carrano, A. L., Lemaster, R.L (1999). Quantification of process parameters in a wood sanding process. Forest Prod. J. 49(5): 41-46

56. Terry, A., Brown, C. (1997). A Comparison of topographic characterization parameters in grinding. Annals of CIRP 46/1: 479-500.

57. Ulf, P. (1998). In-process measurement of surface roughness using light scattering. Wear. Vol. 215. pp. 54-56.

58. U.S. Department of Commerce. (1967). Grading of abrasive grain on coated abrasive products. Standard PS8-67. National Bureau of Standards. 36 pp.

59. Weissberg, R., Buker S. (1990). Writing up Research. Prentice-Hall, Englewood Cliffs, New Jersey.

60. Whitehouse, D. J., Bowen, D. K, Venkatesh, V.C. (1994). Gloss and Surface Topography. CIRP Annals – Manufacturing Technology, V 43, n2, pp 541-549.

61. Zhang, L.C., Yasunga, N. (1997). Advances in Abrasive Technology. World Scientific Press. Sydney, Australia.

APPENDICES

APPENDIX A

Noise matrix data:

Following is the data obtained as a result of the noise matrix analysis carried out to determine the effects of individual parameters on surface roughness.

Table 9-1: Data of individual effect of number of pyramids on roughness parameters.

Matrix	Ra	Rq	Rsk	Rku	Rp	Rv	Rt = Rp+Rv	Ry	Rz
1 X 1	9.66	11.21	-1.11	2.60	22.35	11.51	33.86	34.70	33.87
2 X 2	10.18	11.55	0.04	1.60	25.84	8.40	34.24	34.84	34.24
4 X 4	9.40	11.07	0.72	2.17	28.27	6.09	34.36	35.00	34.37
6 X 6	7.70	10.00	1.39	3.76	30.52	4.50	35.02	37.70	35.01
7 X 8	5.40	7.74	1.90	6.19	30.03	3.29	33.32	35.60	33.33
9 X 10	3.67	5.44	2.42	10.11	25.88	2.42	28.30	34.25	28.30
12 X 11	3.07	4.51	2.41	10.48	23.42	2.02	25.44	29.00	25.45
13 X 13	2.23	2.98	1.73	7.72	14.95	1.56	16.51	19.90	16.52
15 X 15	1.86	2.31	0.94	3.43	9.65	1.31	10.96	11.32	10.96
17 X 17	1.71	2.14	1.03	3.80	9.71	1.18	10.89	11.32	10.90
19 X 19	1.56	1.95	1.07	3.99	9.60	1.07	10.67	11.24	10.68

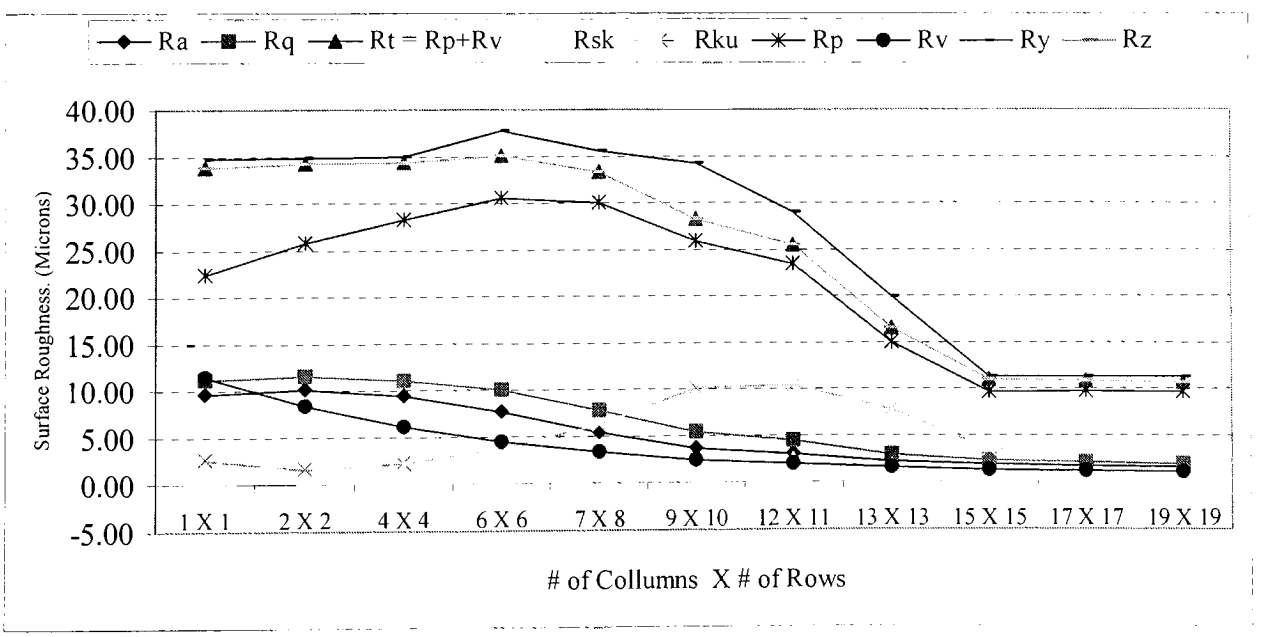

Fig 9-1: Individual effect of number of pyramids on roughness parameters.

Table 9-2: Data of individual effect of sampling resolution on roughness parameters.

Resolution (Microns)	Ra	Rq	Rsk	Rku	Rp	Rv	Rt = Rp+Rv	Ry	Rz
0.10	8.28	10.18	1.08	2.96	26.86	4.89	31.75	34.62	31.75
0.15	8.25	10.13	1.07	2.93	26.60	4.88	31.48	34.26	31.48
0.20	8.24	10.11	1.07	2.93	27.00	4.89	31.89	35.05	31.88
0.25	8.26	10.14	1.07	2.94	27.16	4.89	32.05	36.00	32.05
0.30	8.29	10.19	1.08	2.97	27.00	4.90	31.90	34.08	31.87
0.35	8.28	10.18	1.08	2.96	26.86	4.90	31.76	34.62	31.75
0.40	8.25	10.13	1.07	2.90	26.58	4.88	31.46	34.16	31.46
0.45	8.31	10.23	1.09	3.00	26.81	4.90	31.71	34.60	31.71
0.50	8.28	10.18	1.08	2.96	26.84	4.89	31.73	34.62	31.78

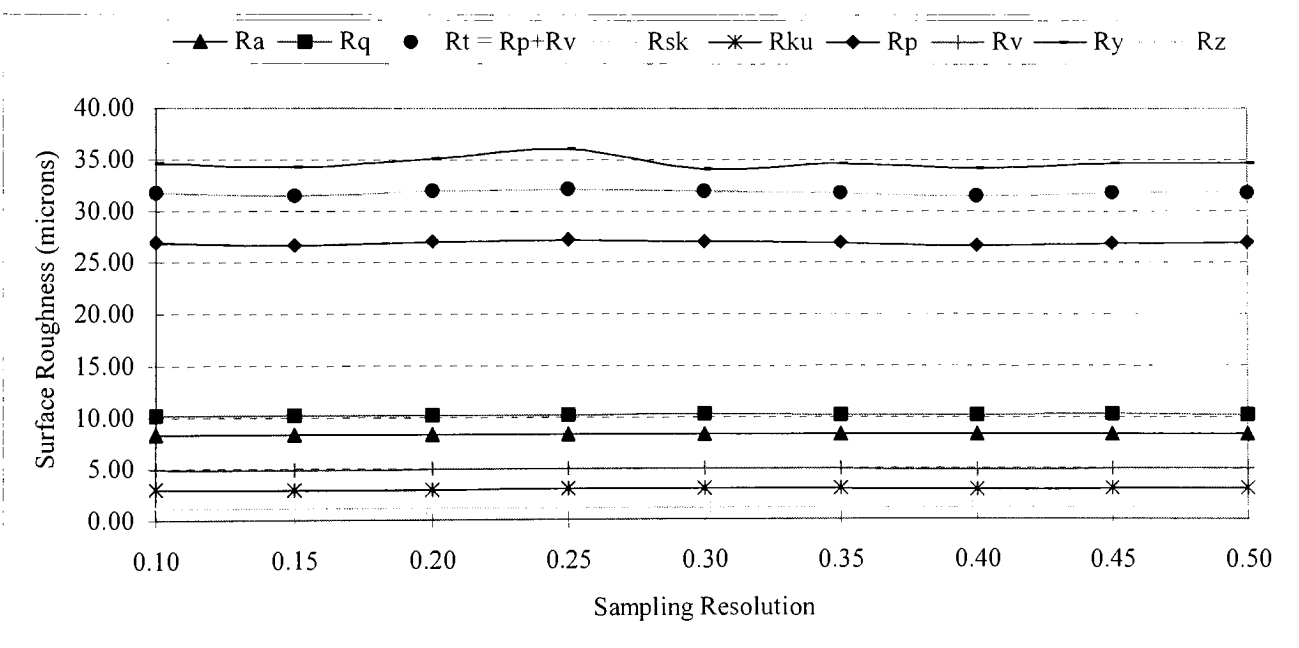

Fig 9-2: Individual effect of sampling resolution on roughness parameters.

Table 9-3: Data of Individual effect of indentation depth on roughness parameters.

Indentation Depth (microns)	Ra	Rq	Rsk	Rku	Rp	Rv	Rt = Rp+Rv	Ry	Rz
10	3.06	3.40	-0.34	1.65	7.23	2.76	9.99	10.74	10.00
15	4.71	5.25	0.12	1.50	11.28	3.54	14.82	15.62	14.82
20	6.10	6.97	0.48	1.77	16.14	4.08	20.22	20.60	20.23
25	7.12	8.36	0.72	2.11	20.14	4.51	24.65	25.08	20.66
30	7.85	9.46	0.93	2.57	24.05	4.77	28.82	32.00	28.83
35	8.33	10.26	1.10	3.02	27.62	4.92	32.54	36.05	32.54
40	8.69	10.95	1.26	3.61	30.96	5.01	35.97	40.18	35.98
45	8.85	11.27	1.36	4.00	33.00	5.05	38.05	43.75	38.06
50	9.02	11.66	1.48	4.58	36.42	5.10	41.52	49.58	41.53

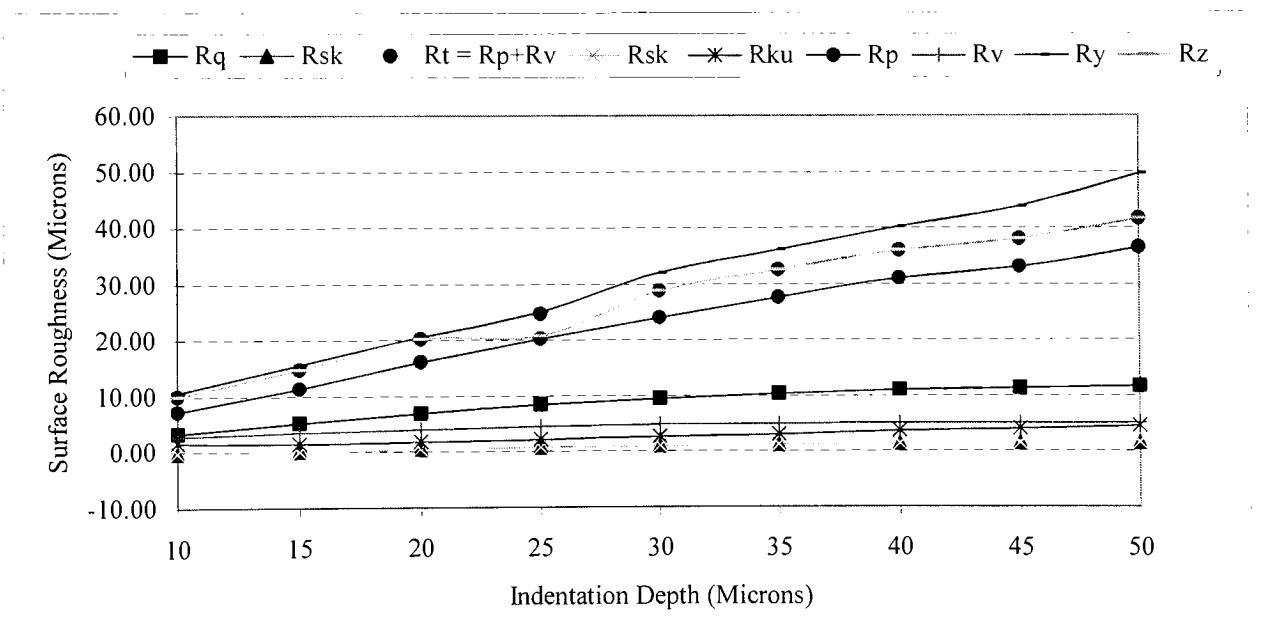

Fig 9-3: Individual effect of indentation depth on roughness parameters.

Table 9-4: Data of individual effect of pyramid height on roughness parameters.

Pyramid Height (Microns)	Ra	Rq	Rsk	Rku	Rp	Rv	Rt = Rp+Rv	Ry	Rz
100	2.18	2.83	1.52	4.77	9.19	1.23	10.42	12.92	10.42
200	4.36	5.66	1.52	4.77	18.38	2.46	20.84	25.85	20.84
300	6.50	8.38	1.46	4.48	25.92	3.68	29.60	35.28	29.61
400	8.08	9.98	1.12	3.09	27.08	4.75	31.83	34.86	31.83
500	9.21	11.01	0.87	2.41	27.29	5.64	32.93	34.65	32.94
600	9.90	11.52	0.65	2.00	27.67	6.36	34.03	34.74	34.03
700	10.34	11.81	0.47	1.74	26.97	6.97	33.94	34.26	33.94
800	10.75	12.13	0.34	1.60	26.85	7.54	34.39	34.80	34.40
900	10.96	12.26	0.20	1.52	26.59	8.04	34.63	35.06	34.64
1000	10.80	11.99	0.05	1.47	25.38	8.33	33.71	33.95	33.72

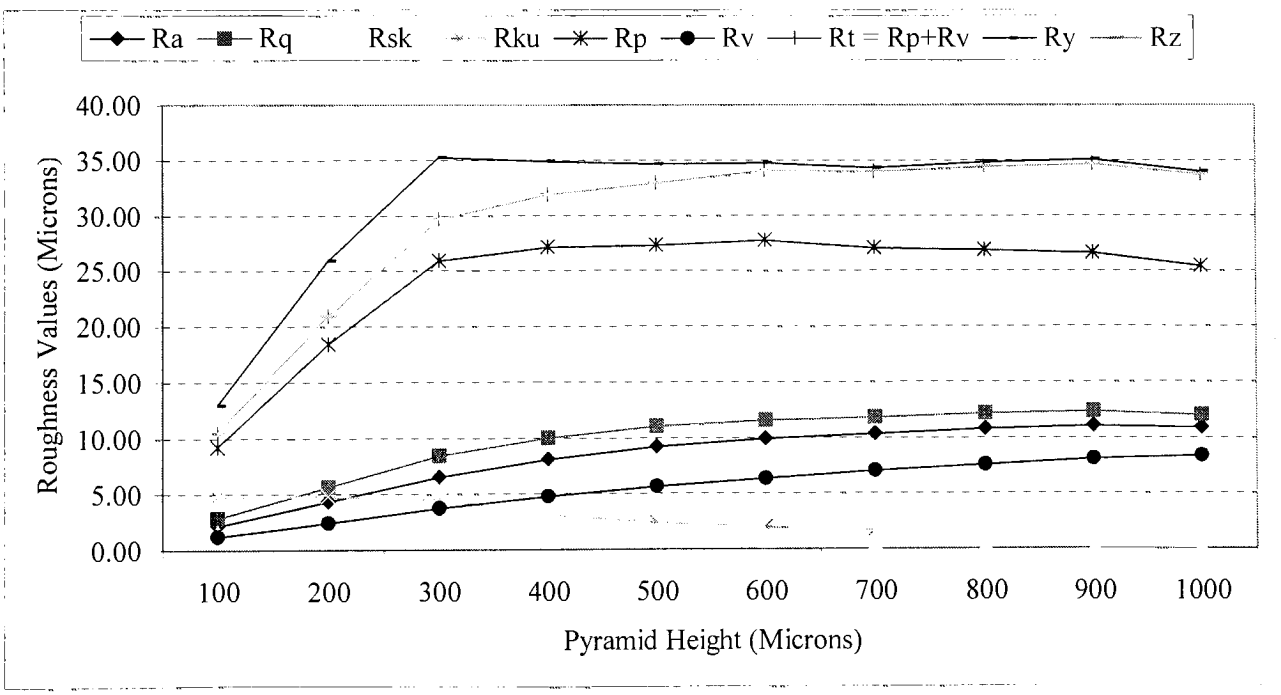

Fig 9-4: Individual effect of pyramid height on roughness parameters.

Table 9-5: Data of individual effect of attack angle on roughness parameters.

Attack Angle (Deg)	Ra	Rq	Rsk	Rku	Rp	Rv	Rt = Rp+Rv	Ry	Rz
0	2.33	5.19	-4.36	22.04	19.78	14.92	34.71	34.84	34.71
5	6.84	8.40	0.71	2.82	24.50	5.52	30.02	34.40	30.02
10	9.03	10.78	0.73	2.28	28.09	5.65	33.74	35.14	33.74
15	9.21	10.92	0.60	2.10	28.74	6.08	34.83	36.57	34.83
20	8.32	10.02	0.76	2.50	27.86	6.00	33.86	34.83	33.86
25	9.31	11.00	0.76	2.30	28.76	6.06	34.83	36.82	34.83
30	5.48	7.13	1.25	4.33	27.76	3.93	31.70	34.04	31.70
35	8.25	10.11	1.06	2.92	27.00	4.88	31.85	35.00	31.85
39	10.11	11.37	-0.48	1.78	23.01	9.25	32.35	34.06	32.35

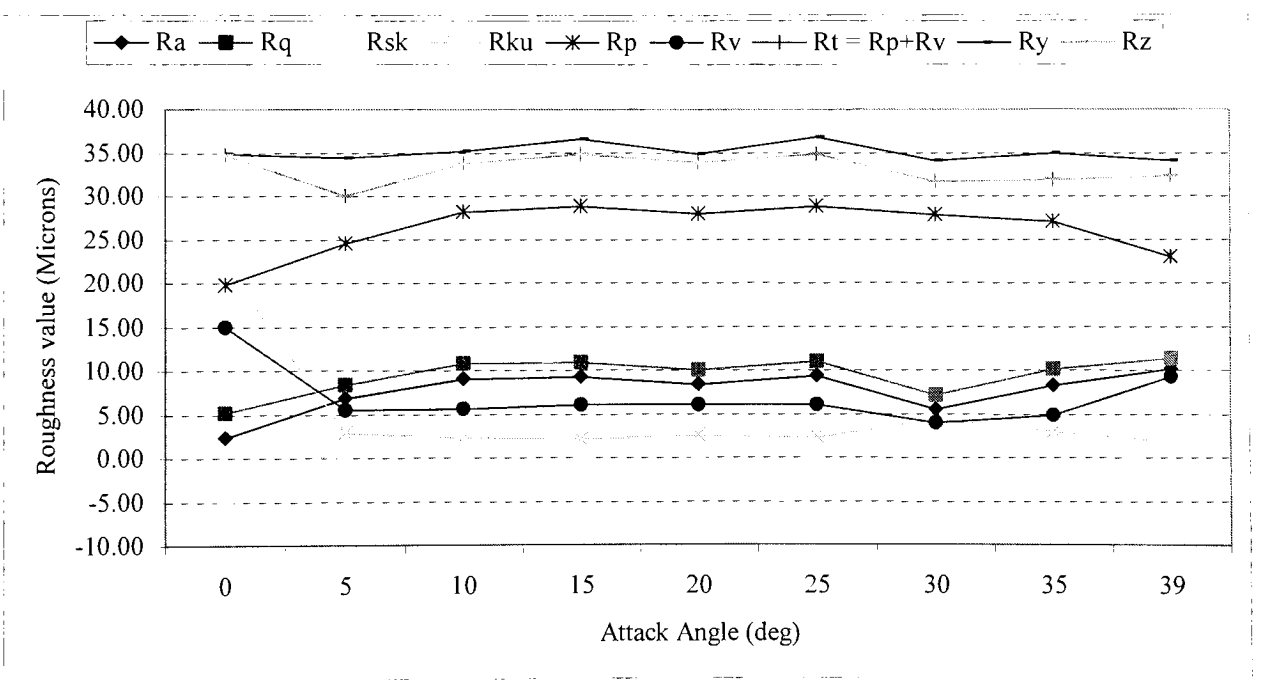

Fig 9-5: Individual effects of attack angle on roughness parameters.

APPENDIX B

Runge phenomenon

Polynomial interpolation is simple, unique, and has a nice geometric interpretation. The polynomial oscillates when the number of interpolation points are fairly large and equidistant. This problem is known as the Runge's Phenomenon.

Example:

The function *f,* whose graph is the continuous curve shown in Figure 9-6 is approximated in two different ways by a polynomial of degree 10 in the interval [-1,1].

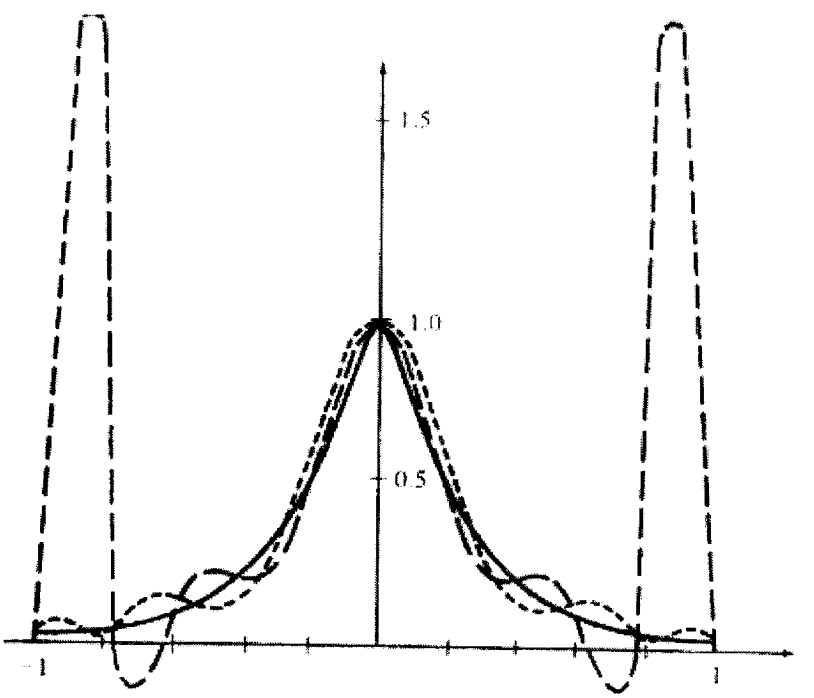

Fig. 9-6: Runge phenomenon

The dashed curve has been determined by interpolation on the equidistant net with eleven points (m=10)

$$x_i = -1 + \frac{2i}{m}, \qquad (i= 0,1,2,.....,m)$$

The graph of the polynomial so obtained has unlike the graph of *f*- a disturbing course between the net points. The agreement with *f* near the ends of the interval is especially bad, while near the center of the interval [-1/5, 1/5] the agreement is fairly good. Such behaviour is typical of *equidistant interpolation with polynomials of high degree*, and can be explained theoretically (**Runge's phenomenon**).

The dotted curve has been determined by interpolation in the so-called **Tchebycheff abscissae**,

$$x_i = \cos\frac{2i+1}{m+1}\frac{\pi}{2}, \qquad i = 0,1,2,.....,m, \quad (m = 10)$$

The agreement with f is now much better than with equidistant interpolation, but still not good. The function is not at all suited for approximation by one polynomial over the entire interval. Here one would get a much better result using approximation by rational functions (somewhat of a trick, since the curve shown is the graph of $f(x) = 1/(1+25x^2)$), or with piecewise polynomials.

Notice that the difference between the values of the two polynomials is much smaller at the net points themselves ($x_i = -1 + 2i/10$) than in certain points between the net points, especially in the outer parts of the interval. This intimates that the values which one gets by equidistant interpolation with a polynomial of high degree can be very sensitive to disturbances in the given values of the function. Put another way: *equidistant interpolation using polynomials of high degree is in some cases an ill conditioned problem, especially in the outer parts of the interval* [x_o, x_m]. The effect is even worse if one extrapolates – i.e., if one computes values of the polynomial at the points outside the net. However, equidistant interpolation works well near the center of the interval.

Even with the equidistant data one can often get a more well-behaved curve by – instead of interpolating – fitting a polynomial of lower degree (e.g., n = 6) using the method of least squares. Generally, if one chooses $n < 2\sqrt{m}$, then the polynomial fit is quite well-conditioned, but higher values of n should be avoided. In the above example, however, the agreement would still be quite bad, even at the net points, when the degree is chosen to be so low.

If one intends to approximate a function *in the entire interval* [-1,1] by a *polynomial* and can choose the points at which the function is computed or measured, then one should choose the *Tchebycheff abscissae*. Using these points, interpolation is a fairly *well conditioned* problem in the entire interval and one can conveniently fit a polynomial of lower degree than *m*, if one wishes to smooth errors in measurement. The risk for disturbing surprises between the net points is significant.

Above example shows how important it is to study the course of the curve $y = f^*(x)$ between those points which are used in the calculations before one accepts the approximation. When one uses procedures for approximation for which one does not have a complete theoretical analysis, one should make an *experimental perturbation calculation*. In the above case such a calculation would very probably reveal that the interpolation polynomial reacts quite strongly if the values of the function are disturbed by small amounts, say $\pm 10^{-3}$, where the sign is chosen randomly (for example, using random numbers generated by the computer). This would give a basis for rejecting the unpleasing dashed curve in the example, even if one knew nothing more about the function than its values at the equidistant net points.

APPENDIX C

Fundamentals of surface roughness and its descriptors.

- **Profiles**

Profiling method: A surface scanning measurement technique that produces a two-dimensional graph or profile of the surface irregularities as measurement data.

Profile: The curve of intersection of a normal plane with the surface.

Nominal profile: A profile of the nominal surface: a straight line or smooth curve.

Real profile: A profile of the real surface.

Measured profile: A representation of the real profile obtained by a measuring instrument. The profile is usually drawn in an x-z coordinate system.

Roughness profile: The modified profile obtained by filtering to attenuate the longer spatial wavelengths associated with waviness.

Mean line: The reference line about which the profile deviations are measured.

Profile peak: The point of maximum height on a portion of a profile that lies above the mean line and between two intersections of the profile with the mean line.

Profile valley: The point of maximum depth on a portion that lies below the mean line and between two intersections of the profile with the mean line.

Roughness sampling length (l): the nominal surface interval within which a surface roughness parameter is determined.

Evaluation length: The length over which the values of surface parameters are determined.

Traversing length: The length of a profile, which I traversed by a profiling instrument to establish a representative evaluation length. Because of end effects in profile measurements, the traversing length must be longer than the evaluation length.

- **Roughness height parameters**

Roughness average (Ra): The arithmetic average of the absolute values of the profile height deviations recorded within the evaluation length and measured from the mean line.

$$R_a = \left(\frac{1}{L}\right)\int_0^L |Z(x)|dx$$

Root mean square (rms) roughness (R_q): The root mean square average of the profile height deviations taken within the evaluation length and measured from the mean line.

$$R_q = \left[\left(\frac{1}{L}\right)\int_0^L Z(x)^2 dx\right]^{\frac{1}{2}}$$

Maximum profile peak height, (R_p): The distance between the highest point of the profile and the mean line within the evaluation length.

Maximum profile valley depth (R_v): The distance between the lowest point of the profile and the mean line within the evaluation length.

Maximum height of the profile (R_t): The vertical distance between the highest and the lowest point of the profile within the evaluation length.

$$R_t = R_p + R_v$$

- **Shape parameters and functions**

Skewness (Rsk): A measure of asymmetry of the profile about the mean line.

$$R_{sk} = \frac{1}{R_q^3}\frac{1}{L}\int_0^L Z^3(x)dx$$

Kurtosis (Rku): A measure of peakedness of the profile about the mean line.

$$R_{ku} = \frac{1}{R_q^4}\frac{1}{L}\int_0^L Z^4(x)dx$$

APPENDIX D

Table 9-6: Final Results after 10,000 iterations for 35 deg attack angle (2D).

Ra	Rq	Rsk	Rku	Rv	Ry	Rp	Rz
3.39	*5.03*	*2.47*	*10.55*	*2.24*	*35.00*	*24.49*	*26.73*

Table 9-7: Final Results after 10,000 iterations for 35 deg attack angle (3D).

Ra	Rq	Rsk	Rku	Rv	Ry	Rp	Rz
3.38	*5.02*	*2.45*	*10.43*	*2.24*	*33.93*	*24.13*	*26.38*

Table 9-8: Final Results after 10,000 iterations for 0 deg attack angle (2D).

Ra	Rq	Rsk	Rku	Rv	Ry	Rp	Rz
2.65	*5.51*	*2.47*	*19.14*	*14.96*	*36.32*	*20.05*	*35.01*

Table 9-9: Final Results after 10,000 iterations for 0 deg attack angle (3D).

Ra	Rq	Rsk	Rku	Rv	Ry	Rp	Rz
3.35	*6.02*	*-3.37*	*16.06*	*14.96*	*38.50*	*20.96*	*35.92*